REMEDY
Et BegrensSkade prosjekt

BegrensSkade/REMEDY

Risk Reduction of Groundwork Damage

Deliverable 4.2

Vibration induced damage due to construction work – Blasting tests

Work Package 4 – Vibrations due to construction activities

Work Package Leader:
Karin Norén-Cosgriff
NGI

Revision: 1

12 / 2021

REMEDY
Et BegrensSkade prosjekt

Note about contributors

Lead partner responsible for the deliverable:	NGI
Deliverable prepared by:	NGI
Other contributors:	Multiconsult, National Public Road Authority

Project information

Project period:	1. September 2017 – 21. August 2022
Web-site:	www.ngi.no/nor/Prosjekter/BegrensSkade-II-REMEDY-Risk-Reduction-of-Groundwork-Damage
Project partners:	Norwegian Geotechnical Institute, Norway (p.nr. 20170774) Sintef Norwegian University of Science and Technology Norconsult Geovita Multiconsult Rambøll Hallingdal bergboring Entreprenørservice Keller Kynningsrud Jetgrunn Skanska Veidekke Finans Norge Huth & Wien Engineering National Public Road Authority (Statens Vegvesen) National Railroad Authority (Bane NOR)

REMEDY
Et BegrensSkade prosjekt

Acknowledgements
Research Funding organizations

Summary

Construction activities such as blasting, piling, compaction, excavation, and construction traffic can produce vibrations of enough strength to cause damage to neighbouring buildings and structures. Guideline limit values for construction vibrations are set in Norwegian Standards. However, building damages assumed to originate from vibrations are seldom observed. This may indicate that today's limit values are unnecessarily strict. A lot of research on how high vibration buildings can tolerate without damage was performed in the 50's - 70's, especially in Sweden and in North America. The limit values used in many countries today are based on these studies. However, the results were affected by the fact that instrumentation and analysis method at that time were less versatile and reliable compared to today's standard. Little newer research has been done, and there is particularly a lack of information about which role the frequency of the vibration plays.

In this study, two instrumented blast test series were performed in a rock quarry in Norway. For the first test series, two buildings were erected, one made of Light Expanded Clay Aggregate (Leca) blocks, and one in cast-in-place unreinforced concrete. Both buildings were founded on a thin compacted gravel layer over rock. In the second test series one building made of Leca blocks was erected on top of an about 4 m thick filling, established at the same location as the buildings in the first test series. The test buildings were instrumented with triaxial geophones, accelerometers and Fiber Bragg Grating Sensors (strain sensors) in multiple positions. To gain full control, repeatability and traceability of the blasts, packaged emulsion and NG-based explosives together with electronic detonators were used.

Several blasts rounds were fired at both test series. The blasts were designed to give increasing vibration values starting at low values and ending at vibration values more than five times above the vibration limit values determined according to today's Norwegian standard, NS8141:2001, which are 50 mm/s for the two test buildings in the first test series and about 20 mm/s for the test building in the second test series. The maximum measured strain levels in the building walls were well above critical strain levels reported in earlier studies. Despite this, no visible damage was detected in any of the buildings.

The results indicate that today's limit values in Norway include a large safety margin for buildings on rock as well as on compacted stiff soil, when considering damage to outer walls, which this study was designed to investigate. However, inner division wall and ceiling material are often the most vibration sensitive parts of the building, especially old plaster and lath walls. This needs to be taken into consideration before the limit values may be adjusted.

Contents

Review and reference page

1 Introduction

Construction activities such as blasting, piling, compaction, excavation, and construction traffic can produce vibrations of enough strength to cause damage to neighbouring buildings and structures. Limit values for vibration from construction work are given in Norwegian Standards. However, building damages assumed to originate from vibrations are seldom observed. This may indicate that today's limit values are unnecessarily strict. The determination of true limit values is very important since they restrict the efficiency of the blasting process, and hence, strict limit values can delay the progress and increase the costs. Little newer research has been done, and there is particularly a lack of information about which role the frequency of the vibration plays.

For this reason, two instrumented blast tests were performed in Spulsåsen rock quarry in Våler municipality in Hedmark, Norway, in November 2018 and November 2020. The tests were conducted in cooperation with the upper secondary school, Solør VGS. The school's personnel and students performed the drilling and blasting with support from the explosive supplier, Austin Norway. The measurements were carried out by NGI and Multiconsult. The executions of the tests were performed within a separate project financed by NPRA Directorate of Public Roads (Statens Vegvesen Vegdirektoratet), National Railroad Authority (Bane NOR), Norwegian Association of Heavy Equipment Contractors (MEF), The Norwegian Defence Estates Agency (Forsvarsbygg) and Norwegian Contractors Association (EBA). However, all data interpretation and reporting have been performed within the Remedy project.

2 Description of test site and buildings

In the first blast test, two test buildings were erected at the site, one in cast-in-place concrete and one made of lightweight construction blocks. Both were founded on an approximately 500 mm leveled and compacted layer of gravel, over rock. The dimensions of both buildings were 5 x 2 x 2.4 (l x w x h) meter. The buildings had one door opening and one window opening each. The two test buildings were mirrored, so that the door openings were facing each other. Figure 1 shows the test buildings and the test area.

The concrete building had 200 mm thick concrete walls without reinforcement, on top of a 400 mm wide wall footing of reinforced concrete. The walls and footing were cast-in-place with C30 grade concrete. The concrete was allowed to cure for 30 days before the blast experiments were performed. The lightweight construction block building was constructed from 250 mm Leca blocks (lightweight expanded clay aggregate) with plastered outer surfaces. This building was founded on top of a wall footing made from 330 mm wide Leca foundation blocks with reinforcement. Reinforcement was also used above the door and window opening.

In the second blast test, one building made of lightweight construction blocks (Leca) was constructed on top of an about 4 m thick filling, established at the same location as the buildings in the first test series, Figure 2. The test building had one door opening and two window openings and the dimensions were 7 x 3 x 2.4 (l x w x h) meter. The fill was constructed of material from the quarry with properties considered approximately as moraines. The fill was established in layers with careful compaction between each layer.

At the top of all building, joists were laid and filled with crushed rock to simulate the mass and ground pressure from a typical detached house on top of a basement.

As cracks in wall- and floor tiles are a common reason for complaints from neighbors to blast sites, one inner wall of the two Leca buildings were covered with tiles, Figure 1c.

Many newer buildings have basement walls of composite materials (insulated blocks) in which it is difficult to attach vibration sensors. In these cases, measurements are sometimes performed on the wooden cladding. To compare measurements on concrete walls with measurements on cladding, a wooden panel was mounted on one of the corners of the concrete building in the first blast test, Figure 1d. The panel was mounted on studs which were screwed into the concrete wall. To compare measurements on insulated blocks with measurements on standard Leca blocks, two insulated Sundolitt RE45 Ring wall blocks were included in the building in the second blast test, Figure 2b. The Sundolitt RE45 Ring wall blocks consist of elements of expanded polystyrene (EPS) with a 6 mm fiber-reinforced cement-based board on the outside. The elements are put together on the construction site, reinforced horizontally and filled with cast concrete.

Figure 1. First blast test a) Test area (left) and test buildings (right). The casted concrete building is under construction. b) Leca building with plaster on outside. c) Inner wall of Leca building covered with tiles (the outside of this wall was facing the blasting area). d) Wooden panel mounted on one corner of the concrete building facing the blasting area.

a

b

c

Figure 2. Second blast test. a) Test building on top off filling (blast area in front). b) two insulated blocks at the back side of the building. c) Filling under construction

2.1 Vibration limit values for the test buildings

Guideline limit values for vibrations from construction activities are given in the Norwegian Standard NS 8141:2001 [1]. The guideline limit values in NS 8141:2001 are intended to prevent damage and are values that buildings are supposed to withstand through repeated exposures. They contain a good safety margin up against values where one can expect that damages will occur and should therefore not be considered as damage limits.

The vibration measure used in NS 8141:2001 is peak particle velocity (PPV) measured in vertical direction close to the building foundation and without any frequency weighting. The calculated guideline limit values in NS 8141:2001 depends on the ground condition, building category, type of foundation, building material, distance

from building and type of vibration source. Table 1 shows calculated guideline limit values for the test buildings in the two blast tests.

Table 1. Vibration limit values for test buildings according to NS 8141:2001

	First blast test Leca and concrete building		Second blast test Leca building	
	Initial value (mm/s)	20	Initial value (mm/s)	20
Ground condition	Thin compacted layer over rock	2.5	Filling with compacted material	1.8
Building category	Ordinary residential	1	Ordinary residential	1
Type of foundation	On thin compacted layer over rock	1	Strip footing	0.7
Building material	Leca blocks/ Concrete without reinforcement	1	Leca blocks	1
Distance	30 - 7 m	1	48 - 9 m	0.6-0.9
Source	Blasting	1	Blasting	1
Limit value		**50**		**16-23**

2.2 Geological survey and GPS surveying

Before the first blast test the geomatics department of NPRA performed a geological survey of the test site by use of Lidar and Orthophoto from drones. The geological survey showed fine to medium-grained red granitic gneiss containing lenses of amphibolite. The dominating direction of foliations is from the blasting area towards the buildings, Figure 3. In addition, the location of the buildings, sensors and top and bottom of all boreholes were determined by GPS surveying. After the first blast test, core samples were taken from intact rock in front of the test buildings, which were tested by SINTEF Byggforsk. For the direction parallel to the foliations, the tests showed an average velocity of 4260 m/s for compression waves, and 2644 m/s for shear waves, and an average density of 2646 kg/m^3 [1].

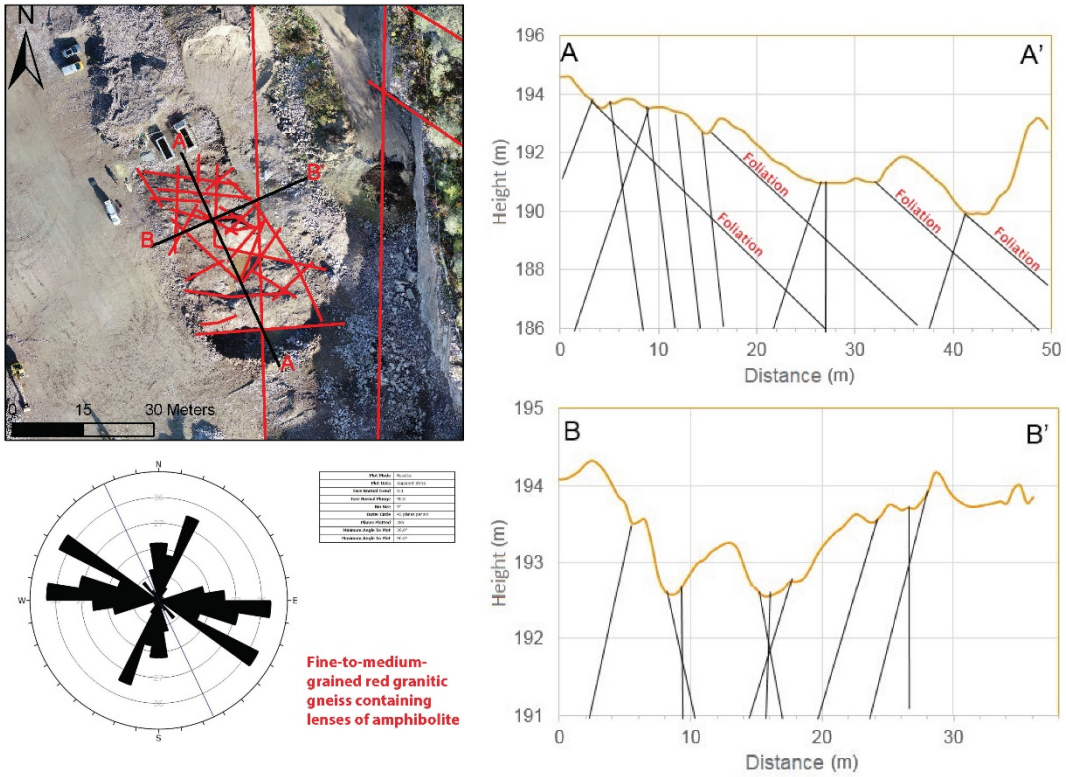

Figure 3. Geological survey of test site.

The shear wave velocity of the filling in the second blast test is estimated by use of the H/V method [3]. According to this method the shear wave speed, Vs, can be estimated as

$$V_s = 4Df \tag{1}$$

where

D is the height of the filling

f is the frequency where there is a distinct peak in the ratio between the frequency spectra of horizontal and vertical velocity measured on the filling, se Figure 4.

Using a filling height of 4 m and a frequency of 13.3 Hz in Eq. 1, the shear wave velocity of the filling is estimated to V_s = 210 m/s.

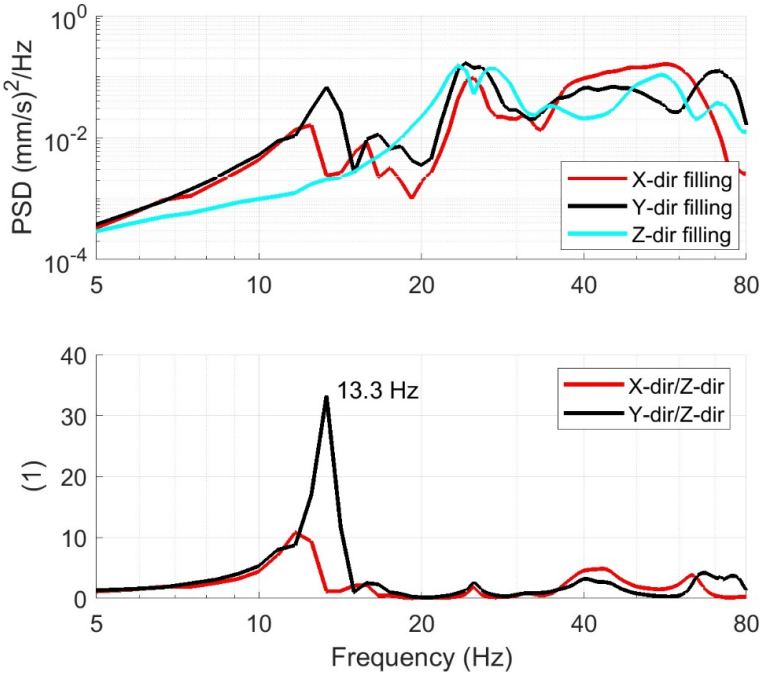

Figure 4. Second blast test. Top: Measured vibration velocity (PSD) in filling in horizontal and vertical direction. Bottom: Ratio between measured vibration velocity in horizontal direction and vertical direction.

3 Instrumentation

Figure 5 - Figure 7 show the instrumentation during the first blast test. Eight three-axial velocity sensors (geophones), four accelerometers and eight strain sensors were mounted on each building. In addition, vertical vibration in three positions on ground and air blast pressure in two positions were measured.

Seven three-axial geophones were mounted on the walls on the short side facing the blasting area and the long side with the door and window opening, Figure 8a. These geophones were either mounted about 20 cm above the footing or 20 cm below the joists. One three-axial geophone was mounted on the long back side of the building about 1 m above the footing. Two vertical geophones were mounted at the bottom of the wooden panel on the concrete house, Figure 8d. Six strain sensors were mounted on the walls in a 45º angle above door openings and above and below window openings and two strain sensors were mounted on the walls over the joints where the short and long walls of the buildings meet, Figure 8b. One microphone for air blast pressure measurement was mounted on the Leca building on the short side facing the blasting area, and one microphone was placed to the left of the Leca building in approximately free field conditions. Three accelerometers were mounted on the walls about 90 cm below the joists on the long back side and one accelerometer was mounted on the tiles on the inside of the short wall facing the blasting area.

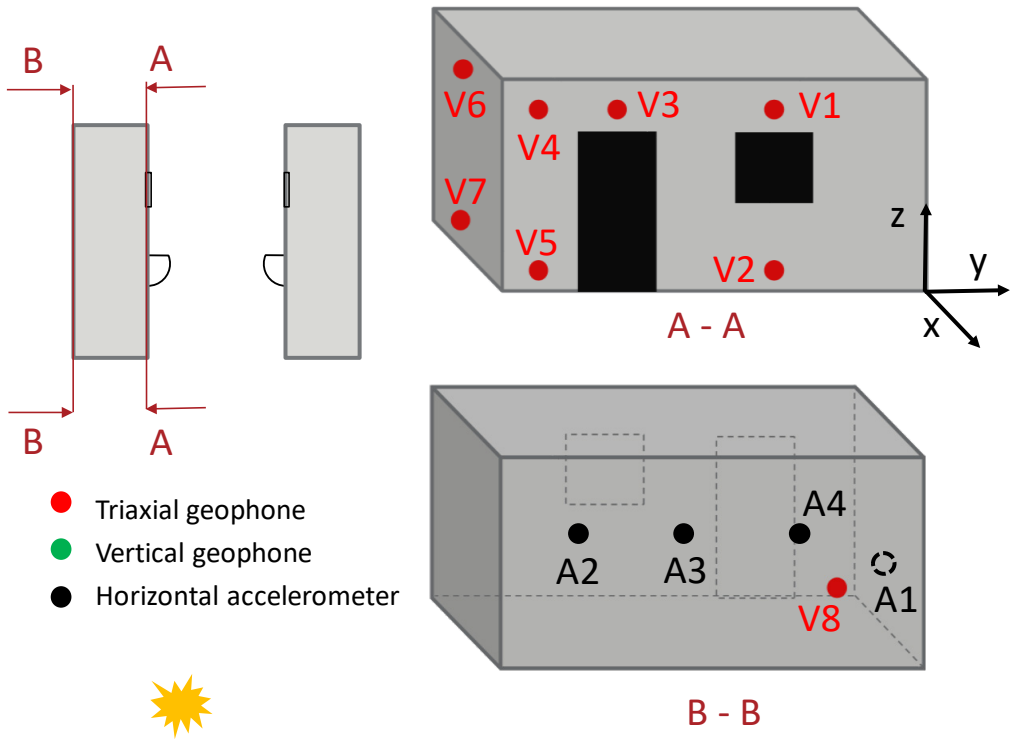

Figure 5. First blast test, instrumentation of test buildings. Position of geophones and accelerometers. Dashed lines illustrate sensor on inside. Sensor positions are identical on the Leca and the Concrete buildings. However, the test buildings are mirrored. Location of the blasting area is marked with a yellow symbol in the left figure.

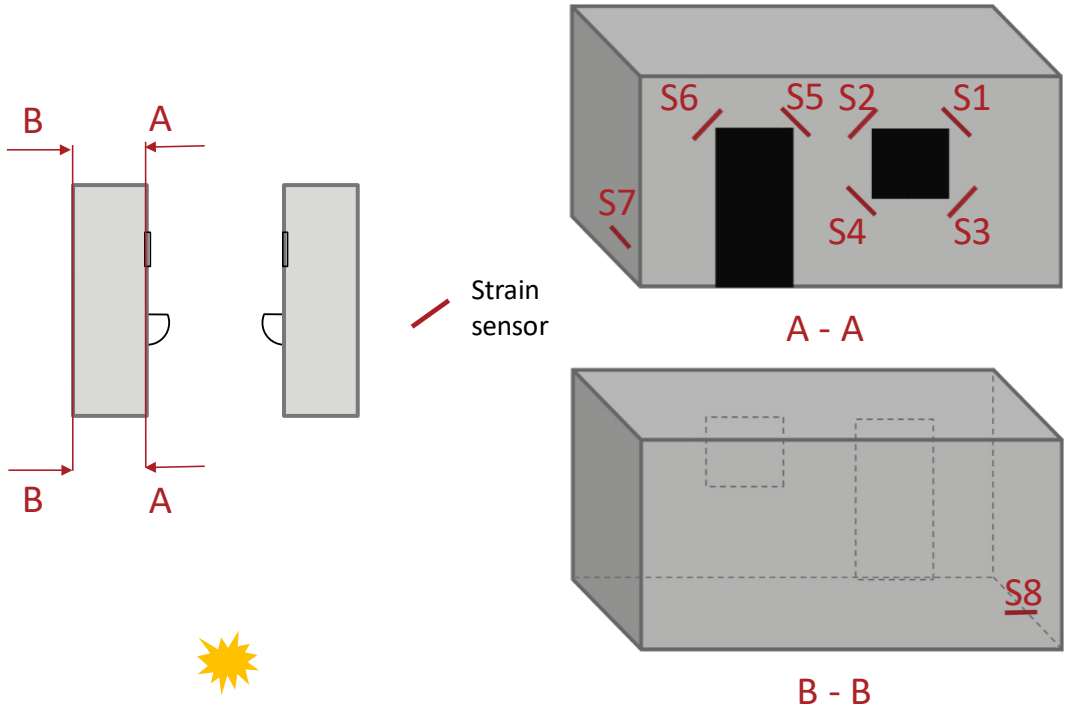

Figure 6. First blast test, instrumentation of test buildings. Position of strain gauges.

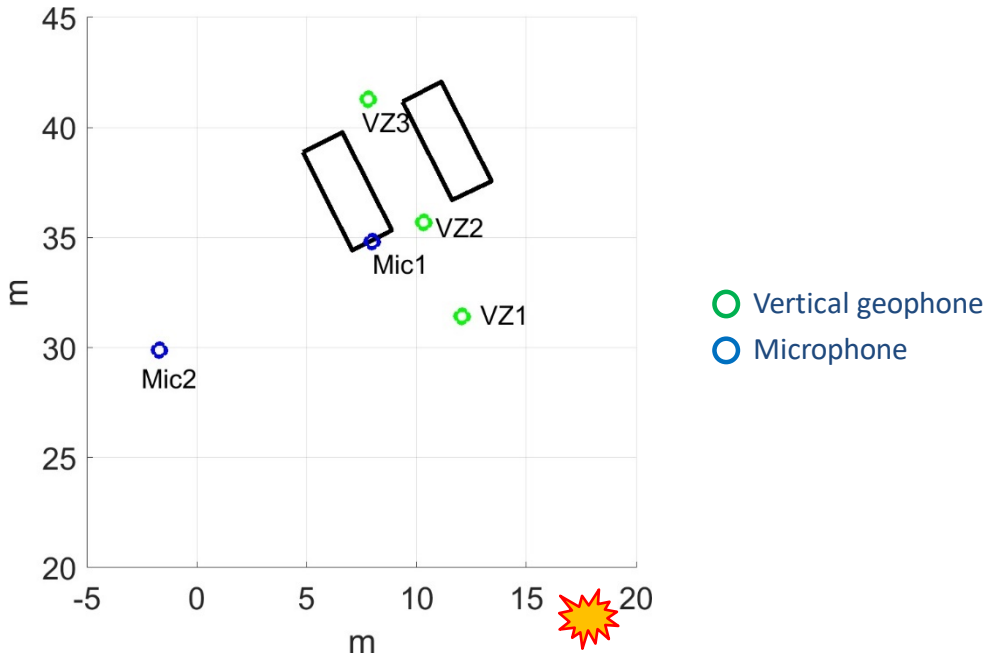

Figure 7. First blast test, instrumentation, position of vertical geophones on ground and air blast microphone on Leca building and in free field.

Figure 8 shows examples of instrumentation used during the two blast tests.

a

b

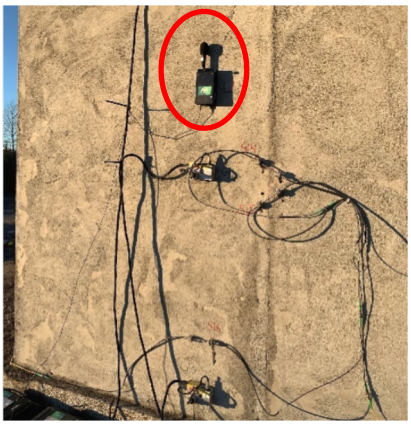

c

d

e

f

Figure 8. First and second blast test, instrumentation. a) Triaxial geophone over door opening. b) Strain sensor over window opening. c) Microphone for air blast pressure (marked with red ring). d) Triaxial geophones on wooden panel (V9) and on the concrete wall on concrete building in first blast test. e) Triaxial geophone and horizontal accelerometer on regular Leca block and vertical geophone and horizontal accelerometer on insulated block in second blast test. f) accelerometer on tiles

Figure 9 - Figure 11 show the instrumentation during the second blast test. 13 three-axial velocity sensors (geophones), 7 accelerometers, 16 strain sensors and one microphone

for air blast pressure were mounted on the walls of the test building. In addition, two three-axial geophones were mounted on top of the filling, two three-axial geophones were mounted on rock behind the filling and one vertical geophone was mounted on rock under the filling. Figure 12 shows numbering and localization of settlement bolts on the buildings four corners and in the filling used for leveling between the blasts.

Eleven three-axial geophones were mounted on the walls either about 12 cm above the footing or about 12 cm below the joists. Two three-axial geophones were mounted in the middle of the short wall facing the blasting area and in the middle of the back wall. One vertical geophone was mounted on the isolated block, Figure 8e. Eleven strain sensors were mounted on long wall with window and door openings and five strain sensors were mounted on the short wall facing the blasting area and on the back wall. One microphone for air blast pressure measurement was mounted on the short side facing the blasting area, Figure 8c. Six accelerometers were mounted on the walls either about 12 cm above the footing or about 12 cm below the joists on the long back side and short side wall facing away from the blasting area. One accelerometer was mounted on the tiles on the inside of the short wall facing the blasting area, Figure 8f.

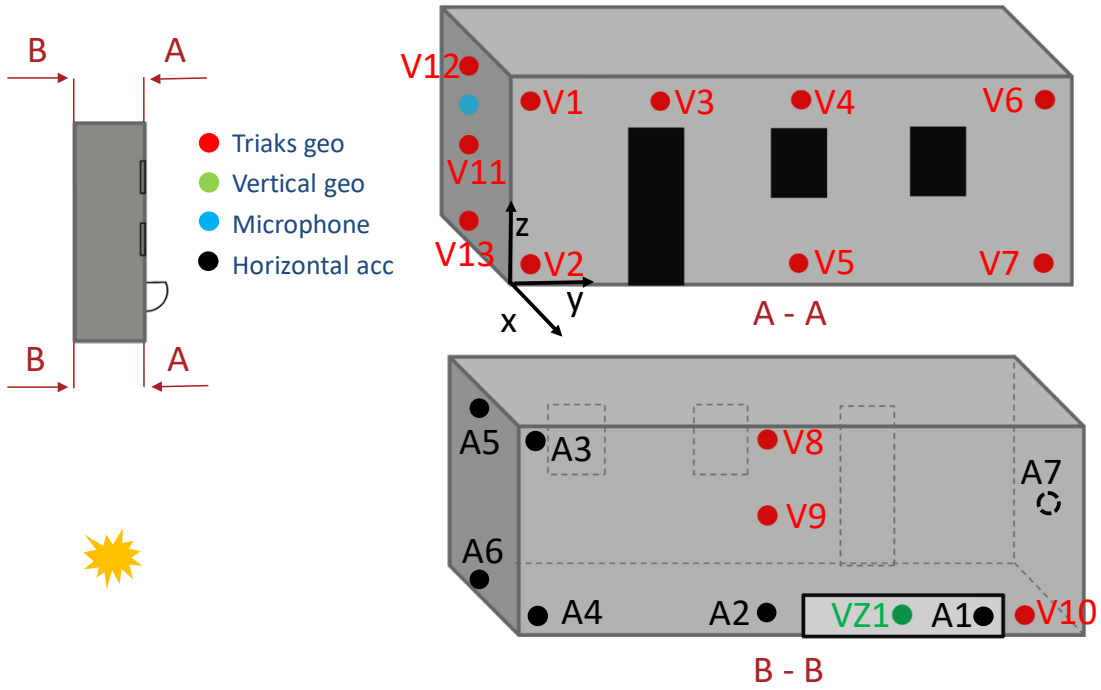

Figure 9. Second blast test, instrumentation of test building. Position of geophones, accelerometers and air blast microphone on test building. Dashed lines illustrate sensor on inside. Location of the blasting area is marked with a yellow symbol in the left figure.

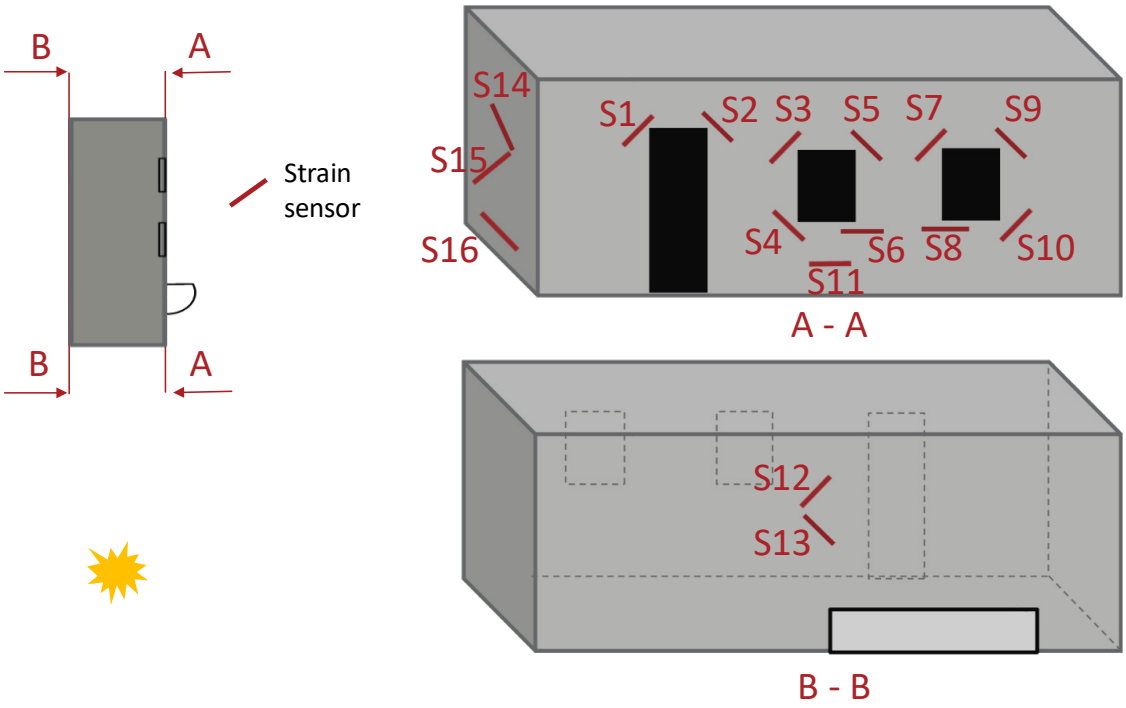

Figure 10. Second blast test, instrumentation of test building. Position of strain sensors on test building. The instrumented short side of the building faces the blasting area.

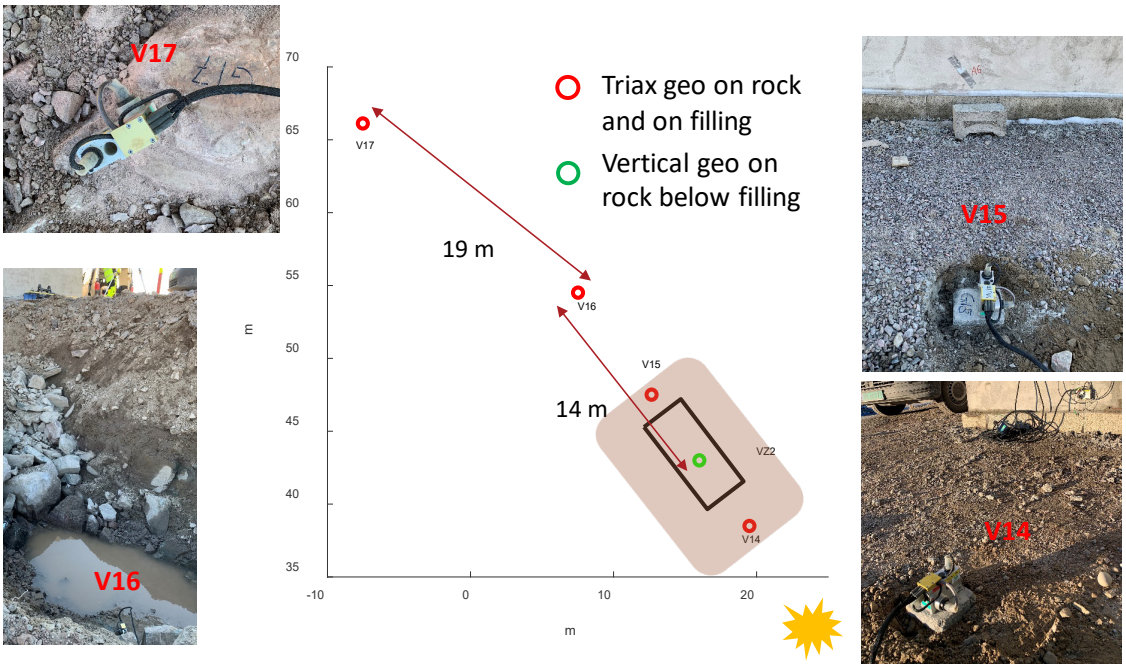

Figure 11. Second blast test, instrumentation on ground.

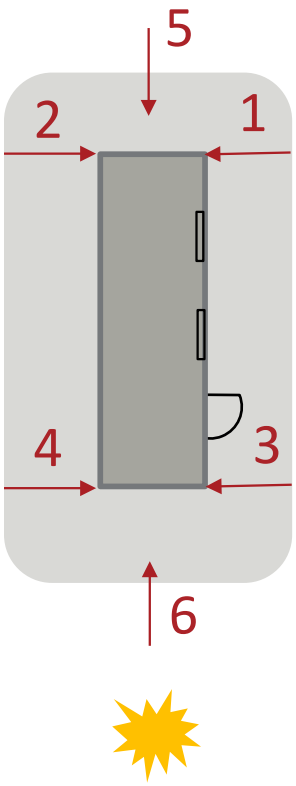

Figure 12. Second blast test, numbering and localization of settlement bolts.

For the geophones and air blast microphone the AVATrace M80 measurement system was used with a 6000 Hz sampling frequency. Each three-axial sensor was connected to its own autonomous four channel logger. The fourth channel of each logger was used as a joint trigger channel. In the first blast test two separate measurement chains were used for the two buildings and the three vertical geophones on ground were divided between the two measurement chains. One vertical geophone in front of each building were used as trigger geophones, ensuring that all measurement channels on each building were mutually synchronized. In the second blast test, all geophones were connected to one measurement chain and a vertical geophone on rock beside the filling was used as a trigger geophone.

For the accelerometer measurements, PCB 308B accelerometers, with a sensitivity of 100 mV/g were used. All accelerometers were connected to the same logger making them mutually synchronized. The sampling frequency was 4096 Hz.

The strain measurements were performed with a fiber optic measurement system from Micron Optics, using os3510 Fiber Bragg Grating Sensors (FBGS) [4]. The strain sensors were attached via rigid brackets bolted to the structures. Dynamic strains were measured over the gage length, of 110 mm. The sampling frequency of the strain measurement system was 1000 Hz. This was considered enough since the frequency content of blast vibration usually are well below 500 Hz. This was also later confirmed

from the vibration measurements. In the first blast test, the sensors measurement range was set to ± 2500 μm, while in the second blast test the measurement range was from about -1800 μm to +3200 μm. The strain sensors were assembled in joint fiber cables, making them mutually synchronized.

The collected time series from all sensors were analyzed in MatLab.

4 Execution of blast tests

The blasts were designed to give increased vibration strength, starting at a low value for the longest distance and increasing progressively as the blasts came closer to the test structures.

To gain full control, repeatability and traceability of the blasts, packaged emulsion and NG-based explosives together with electronic detonators were used, see Figure 13. Drill diameter was 76 mm. The distance between the rows (burden) was about 2.0 m, and the spacing between each hole was about 2.5 m. The maximum borehole depth in each round was between 4.5 – 7 m. A 1.0 - 1.5 m crushed stone stemming was used in all holes (Figure 13). Coordinates for top of all boreholes were determined by GPS surveying before the tests. In the first blast test, coordinates were also determined for the bottom of the holes using a borehole deviation probe.

The buildings were visually inspected between each blast round to detect and document any damage. In addition, the results from the strain measurements were reviewed correspondingly to detect any changes not visible to the naked eye.

In the second blast test, the buildings four corners and the sensors mounted in the filling (sensor 14 and 15) were provided with settling bolts and were leveled before and after each blast round, Figure 13d. The numbering and localization of the settlement bolts are shown in, Figure 12.

a

b

c

d

Figure 13. a) Explosives, b) electronic detonators specifications, c) stemming with crushed rock, d) leveling of building and filling between each blast.

4.1 First blast test

The first blast test was performed from 6th to 9th November 2018. The weather in the measurement period was cloudy with periods with light precipitation. The

temperature was never below 0°C and the average temperature was between 5°C and 6°C.

Five blasts rounds were fired consisting of all together 143 charged holes. The number of holes detonated in one blast round varied from two single holes up to 53 holes. The first four rounds were all shot by single hole initiation, with a delay between each hole in a row of 10 ms, while round five was shot by two and two holes simultaneously starting in the centre of the rows. The delay between the rows varied from 10 ms to 60 ms. The total amount of explosives detonated in one blast round varied from 6.5 to 404 kg, and the explosives detonated per delay varied from 3.0 to 37.8 kg. The blasts were designed to give equal dynamic loading on each of the two test structures. The first blasting round had a minimum distance of 29 m from the test structures, while the last had a minimum distance of 7 m. Figure 14 and Table 2 describes the test setup.

Table 2. First blast test, description of blasts

Blast round	No charged holes	Total charge (kg)	Max charge/ delay (kg)	Min dist (m)		Min square root scaled distance (m/√kg)	
				Leca	Concrete	Leca	Concrete
1	46	222	8.4	28.9	30	11.5	11.2
2.1	1	3	3	29.5	26.7	17.0	15.4
2.2	1	3.5	3.5	26.5	23.5	14.5	12.9
3	53	404	14	17.5	18.5	5.4	5.7
4	22	287	16.4	12.3	13.2	3.2	3.3
5	20	266	37.8	7.4	7.2	1.0	1.1

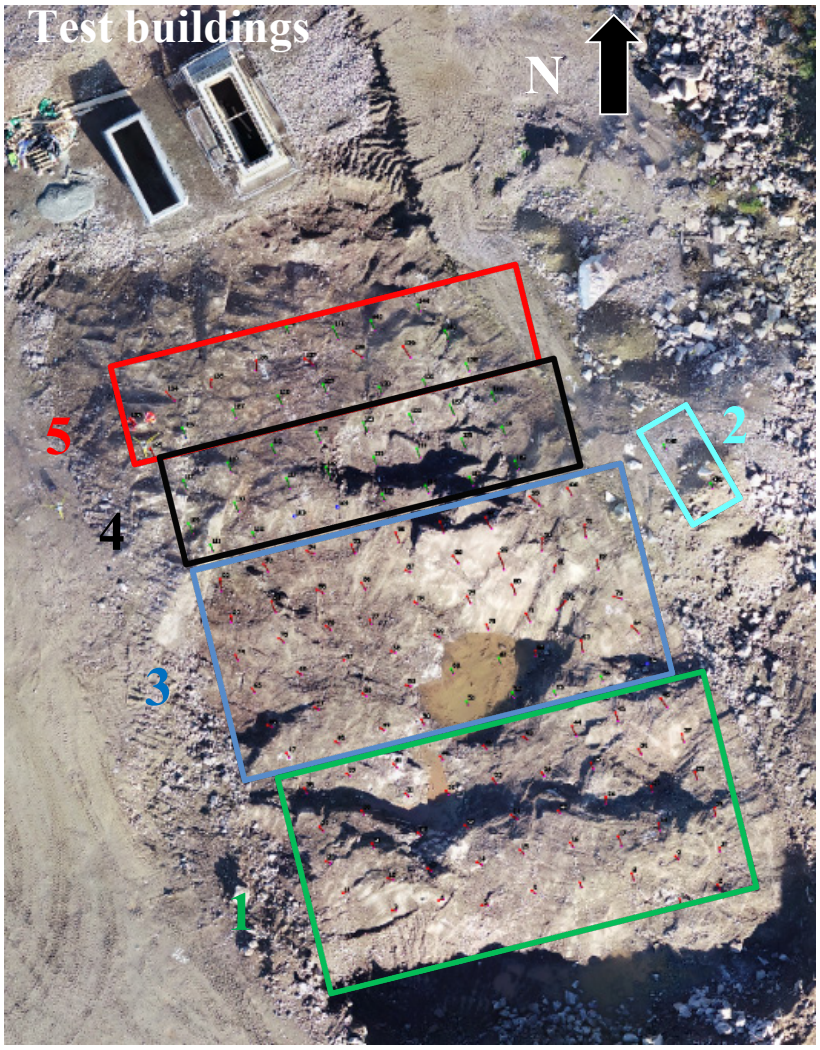

Figure 14. First blast test, localisation and numbering of the blast rounds. Test building in top left corner (Leca on the left and concrete on the right)

To investigate whether the response can be assumed to be dominated by body waves (P- and S-waves) or surface waves, angle of incidence is calculated for all boreholes from the coordinate for the bottom of the boreholes and the coordinates for the closest parts of the buildings. This corresponds to the smallest possible angle, since the explosives are distributed in the boreholes and the angle will be larger for explosives closer to the surface. The calculated angles of incidence are shown in Figure 15 and tabulated in Table 3.

As a role of thumb, the ground surface vibration response to a blast will be dominated by body waves, if the angle between a surface normal through the receiver point and a line from the receiver to the source point (blast), is less than 60 degrees. For larger angles, i.e. larger distances, surface waves will dominate. The calculations show that surface waves can be assumed to dominate the response for blast round 1-3. For blast

round 4 body waves may dominate for some holes in the closest row and for blast round 5 body waves may dominate for most of the boreholes.

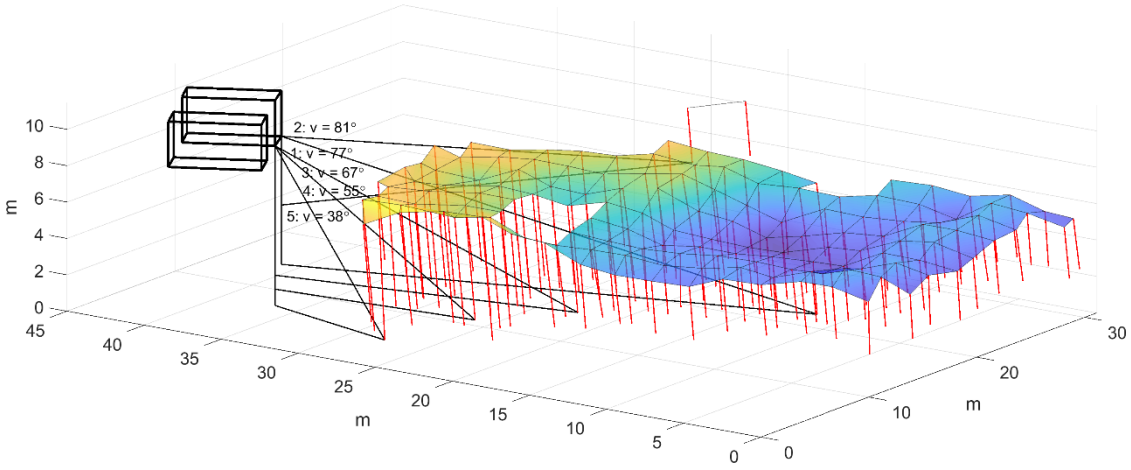

Figure 15. First blast test, plot of test area with test buildings and boreholes (red lines). The minimum incident angle for vibration waves to the buildings are shown for each blast round

Table 3. First blast test, calculated minimum angle of incidence.

Blast round	Angle of incidence (deg)
1	77-81
2	81-82
3	67-79
4	55-70
5	38-65

4.2 Second blast test

The second blast test was performed from 23th to 26th November 2020. The weather 23th – 25th was cloudy with periods with light precipitation, while 26th was cloudless. The temperature in the measurement period was between -2°C and +9°C.

Four blasts rounds were fired consisting of all together 220 charged holes. The number of holes detonated in one blast round varied from three to 98 holes. The first round consisted of three single constricted charges, which were shoot with three seconds in between. The second and third blast rounds were shoot by single hole initiation, with a delay between each hole in a row of 5-10 ms in blast round two, and 2-10 ms in blast round three. In the fourth blast round the last row was shot by three and three holes simultaneously, while the delay between the holes in the other rows was 2-5 ms. The total amount of explosives detonated in one blast round varied from 12 to 1485 kg, and the explosives detonated per delay varied from 2.0 to 47.8 kg. The first blasting round had a minimum distance of 36 m from the test building, while the

last blast round had a minimum distance of 9 m. Figure 16 and Table 4 describes the test setup.

Table 4. Second blast test, description of blasts

Blast round	No charged holes	Total charge (kg)	Max charge/ delay (kg)	Min dist (m) a	Min square root scaled distance (m/√kg)
1.1	1	2.1	2.1	48.3	33.3
1.2	1	4.2	4.2	42.5	20.7
1.3	1	6.3	6.3	36.2	14.4
2	50	611.5	14.6	33.5	8.8
3	98	1485.6	17.2	18.7	4.5
4	69	1026.0	47.8	8.8	1.3

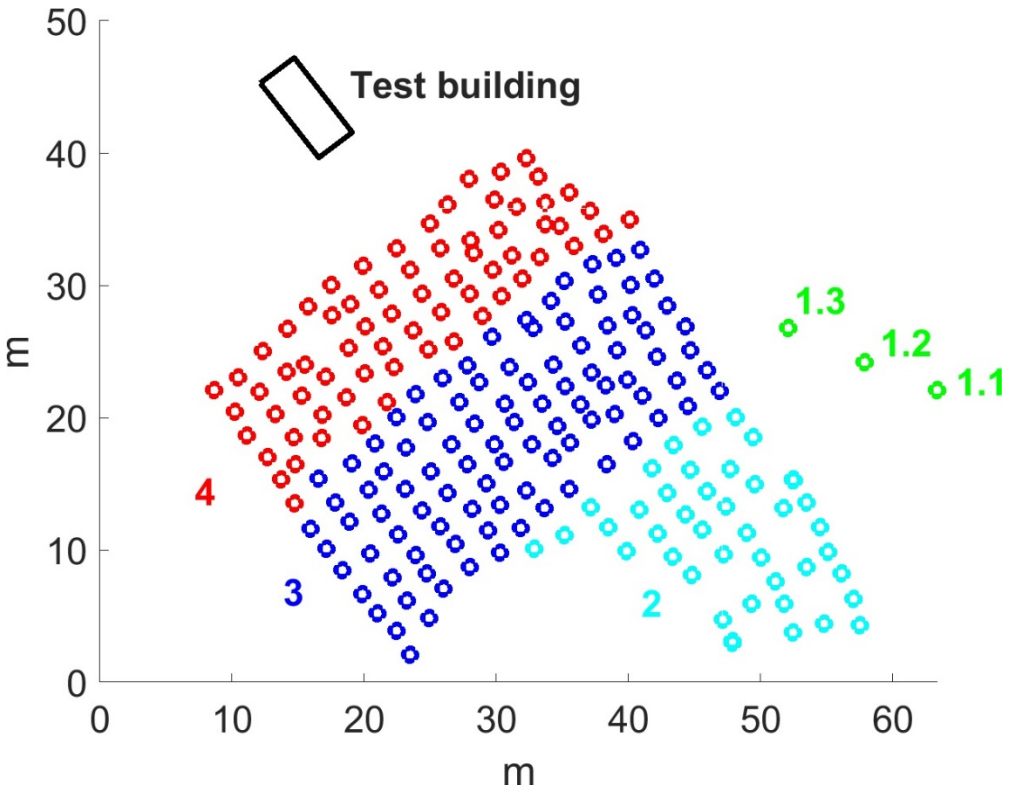

Figure 16. Second blast test, localization and numbering of blasts.

Table 5 shows the results from the levelling between each blast round. See Figure 13e for localization and numbering of the settlement bolts. The leveling shows small settlements of the building corners (1-4 mm). Most of the settlements were induced already after the first blast round and were stable for the following blast rounds. However, the two corners closest to the blast area received increased settlements after the last blast round. The leveling of the sensor in the filling on the back side of the building showed small settlements (1-2 mm). The leveling of the sensor in the filling in

front of the building showed a settlement of about 10-12 mm after the first blast round and no further development thereafter.

Table 5. Second blast test, measured settlements

Change in level from height before blast test, settlement (mm)				
Bolt no	Reading after blast round no			
	1	2	3	4
1	± 2	± 1	± 1	± 2
2	± 2	± 2	± 2	± 2
3	± 2	± 2	± 2	± 4
4	± 3	± 2	± 2	± 4
5	± 2	± 1	± 1	± 1
6	± 12	± 10	± 12	± 10

5 Test results

Table 6, Table 7 and Table 10 show measured PPV, Table 8 and Table 11 show measured peak air blast pressure and Table 9 and Table 12 show measured peak strain during the first and second blast tests.

Table 6. First blast test, Leca building. Measured maximum PPV. Sensor number in parentheses, see Figure 5 for coordinate system and sensor positions. Maximum measured value in vertical direction close to foundation and limit value according to NS 8141:2001 are shown for comparison.

Blast round	PPV (mm/s)				
	X	Y	Z	Close to found, Z	Limit value, Z
1	27 (V1)	26 (V6)	32 (V4)	30	50
2.1	23 (V1)	36 (V6)	42 (V4)	39	
2.2	32 (V5)	39 (V6)	52 (V6)	48	
3	39 (V7)	70 (V6)	89 (V4)	86	
4	71 (V5)	133 (V3)	129 (V6)	119	
5	230 (V5)	233 (V6)	>260 (all)	>260	

Table 7. First blast test, concrete building. Measured maximum PPV. Sensor number in parentheses, see Figure 5 for coordinate system and sensor positions. Maximum measured value in vertical direction close to foundation and limit value according to NS 8141:2001 are shown for comparison.

Blast round	PPV (mm/s)				
	X	Y	Z	Close to found, Z	Limit value, Z
1	22 (V1)	15 (V6)	14 (V7)	14	50
2.1	17 (V3)	16 (V6)	30 (V6)	29	
2.2	16 (V3)	21 (V6)	27 (V6)	26	
3	46 (V3)	53 (V6)	45 (V4)	43	
4	79 (V3)	101 (V6)	81 (V7)	81	
5	>260 (V4)	>260 (V3,V4,V6)	>260 (all)	>260	

Table 8. First blast test, measured peak air blast pressure. See Figure 7 for sensor positions.

Blast round	Peak air blast pressure (Pa)	
	Pos 1, on wall	Pos 2, free field
1	234	119
2.1	0.8	0.8
2.2		
3	339	233
4	425	349
5	750	682

Table 9. First blast test, Leca and concrete building. Measured maximum peak strain, see Figure 6 for sensor positions.

Blast round	Strain (μstrain)			
	Close to foundation on intact wall, sensor S7 and S8		Above door openings sensor S5 and S6	
	Leca	Conc	Leca	Conc
1	14	10	75	17
2	24	7	72	15
3	26	8	159	24
4	41	14	334	40
5	342	34	733	> 1750

Table 10. Second blast test, Leca building. Measured maximum PPV. Sensor number in parentheses, see Figure 9 for coordinate system and sensor positions. Maximum measured value in vertical direction close to foundation and limit value according to NS 8141:2001 are shown for comparison.

Blast round	PPV (mm/s)				
	X	Y	Z	Close to found, Z	Limit value, Z
1.1 [1)]	5 (V4)	4 (V12)	7 (V9)	6	16
1.2 [1)]	7 (V4)	7 (V12)	11 (V8)	11	17
1.3	8 (V8)	15 (V12)	23 (V6)	20	17
2	17 (V9)	21 (V13)	23 (V9)	22	17
3	28 (V4)	51 (V12)	40 (V6)	31	20
4	75 (V3)	112 (V13)	180 (V1)	170	23

1) Sensor 6 and 7 were not connected during this blast

Table 11. Second blast test, measured maximum peak air blast pressure. See Figure 9 for sensor position.

Blast round	Peak air blast pressure (Pa)
1.1	- [1)]
1.2	- [1)]
1.3	- [1)]
2	- [1)]
3	- [1)]
4	437

1) The air blast microphone was malfunctioning during blast 1-3

Table 12. Second blast test, Leca building. Measured maximum peak strain, see Figure 10 for sensor position.

Blast round	Strain (µstrain)			
	On intact walls		Above door and window openings	
	Strain	Pos	Strain	Pos
2	11	S16	34	S7
3	19	S14	87	S1
4	94	S16	> 3200	S2

In the first blast test, the measured vibration and strain values were consistently higher in the Leca building than in the concrete building. The last and closest blast round was however an exception producing vibration values outside the measurement range of the recording system on both buildings (>264 mm/s), and high strains above the doors of the test buildings (especially the concrete building).

In the second blast test, the highest measured PPV was 180 mm/s. The last and closest blast round produced high strains above the door of the test building.

The measured vibration values were well above the guidance limit values for all test buildings. Nevertheless, the blast tests did not result in damage to any of the buildings that could be detected during the inspections after each blast round. However, the last blasts in each test produced a residual strain response, which was not visible to the naked eye. In the first blast test the residual strain above the door on the concrete building was measured to 500 μstrain over the 110 mm long sensor. In the second blast test the residual strain above the door of the test building (Leca building) was measured to 1400 μstrain. If these differential movements were concentrated at one point, they would represent a 0.05 mm and a 0.14 mm change respectively.

5.1 Strain calculated from measured vibration velocity and displacement

The strain levels which the buildings are exposed to can also be estimated from measured vibrations. There are two basic approaches to evaluate strain from measured vibrations: the wave propagation-based approach and the displacement-based approach [5].

In the wave propagation approach, strain is calculated from the ratio of particle velocity to wave velocity. In the displacement-based approach, the measured velocity time series are integrated to displacement time series and the difference between the displacement time series from the different sensors are used to calculate strain time series.

5.1.1 Calculation based on wave propagation

A blast initiates different types of ground waves which propagate with different speeds: relatively fast compression waves, shear waves with about half the speed of the compression waves (unless in saturated lose soils), and surface (mainly Rayleigh-type) waves with slightly slower speed than the shear waves. Different directions of particle velocity and types of wave velocities are used to compute various components of strain. Rayleigh waves appear only down to a depth corresponding to about one wavelength, and decays therefore slower with distance than the other two wave types. Hence, Rayleigh waves dominates already at relatively short distances from the source. In addition, Rayleigh waves have the lowest propagation velocity.

Therefore, Rayleigh waves will cause the highest strains and hence expose buildings to the greatest stresses.

Rayleigh like surface waves involve particle motions both in horizontal and vertical directions. The vertical particle motion of the wave imposes a dynamic shear strain, γ_{xy}, in a building that flexes with the distortion of the ground surface. The shear strain generates a tensile strain at 45 ° angle to the x-y axis of the shear strain:

$$\varepsilon_{xy,max} = \frac{1}{2}\gamma_{xy,max} = \frac{V_{V0}}{2c} \quad (2)$$

The horizontal particle motion imposes a tensile strain in the x-direction, which amount to:

$$\varepsilon_{x,max} = \frac{V_{H0}}{c} \quad (3)$$

In Rayleigh waves the vertical and horizontal wave amplitudes, V_{H0} and V_{V0} are of the same order of magnitude, the ratio between them depends on the ground conditions. By basing the assessment on measured vertical particle velocity – V_{V0}, the maximum tensile strain amplitude a passing Rayleigh-type vibration wave exposes a building to, can reasonably well be estimated to be:

$$\varepsilon_{x,tensile,max} = \frac{V_{v0}}{c} \quad (4)$$

Bending of the building together with the ground when the vibration wave passes can also be a possible damage mechanism. This is especially the case for soft ground conditions when the wave speed is low, and the wavelength of the surface wave can be in the same range as the length of the building. The maximum strain from bending in a building with a height H can be estimated as

$$\varepsilon_{x,bend,max} = \frac{V_{v0}2\pi H}{c\lambda} \quad (5)$$

Where

V_{v0} is the amplitude of the vertical particle velocity
c is the propagation speed of the dominating R-wave, here assumed to be about 2400 m/s.
H is the height of the building
λ is the wave length

Due to the nature of the Rayleigh wave, the vertical and horizontal surface motion components appear 90° out of phase – i.e. the surface particle motion is elliptic. Dynamic strain components based on vertical and horizontal surface motion do therefore appear ¼ wavelength apart and do not act in the same plane. They therefore never add, i.e. the total strain from Eq. 4 and Eq. 5 are to be calculated as

$$\varepsilon_{x,tot,max} = \sqrt{\varepsilon_{x,tensile,max}{}^2 + \varepsilon_{x,bend,max}{}^2} \quad (6)$$

The theory is discussed in more detail and the equations are deduced in [6].

Another possible damage mechanism is amplification of the vibration velocity because of dynamic building response, which occurs when excitation and the building's natural frequencies are close. Note that possible effect of building response is not included in strain calculated according to Eq. 4, 5, and 6

5.1.2 Calculation based on displacement

In the displacement-based approach, strain is assessed from measured vibrations by calculation of difference in displacement time series determined by integration of measured velocity time series. In these calculations, possible effect of building response is included.

Vertical strain, ε_z, and shear strain, γ, are estimated as

$$\varepsilon_z = \frac{\Delta\delta_{z,max}}{h} \quad (7)$$

$$\gamma = \frac{\Delta\delta_{y,max}}{h} \quad (8)$$

where

$\Delta\delta_{z,max}$	is maximum difference in vertical displacement
$\Delta\delta_{y,max}$	is maximum difference in horizontal displacement in y-direction
h	is vertical spacing between sensor

Eq (2) and Eq (8) give the tensile strain from shearing

$$\varepsilon_{zy} = \frac{\Delta\delta_{y,max}}{2h} \quad (9)$$

5.1.3 Calculated strain

Table 13, Table 14 and Table 15 show measured strain and strain calculated based on wave propagation (Eq. 4, Eq. 5 and Eq. 6) and displacement (Eq 7. And Eq. 9). Calculated strains are plotted against measured strain in Figure 17.

In the calculations based on wave propagation, average shear wave velocity in the ground as determined from the laboratory tests, vertical PPVs and frequency measured on the buildings, close to the foundations are used.

In the calculations based on displacement, measurements in position V6 and V7 on the short side (Figure 5) are used in the calculations for the first blast test. Blast

round 5 is excluded in the calculations of vertical strain, since all vertical velocity sensors were out of range in this blast round and integration may give erroneous results. For the second blast test, position V1, V2, V6 and V7 on the long side of the building and position V12 and V13 on the short side are used (Figure 9).

Table 13. First blast test, Leca building. Measured and calculated peak strain.

Blast round	Strain (μstrain)						
	Measured		Calculated based on wave propagation			Calculated from displacement	
	On intact wall	Above door openings	From shear Eq.4	From bending Eq.5	Total strain Eq.6	Vertical from Eq.7	From shear Eq.9
1	14	75	12	7	14	7	15
2.1	19	61	16	6	17	10	18
2.2	22	73	20	8	21	17	21
3	26	159	36	15	39	37	57
4	41	334	49	14	51	389	106
5	342	733	>110	>32	>115		445

Table 14. First blast test, concrete building. Measured and calculated peak strain.

Blast round	Strain (μstrain)						
	Measured		Calculated based on wave propagation			Calculated from displacement	
	On intact wall	Above door openings	From shear Eq.4	From bending Eq.5	Total strain Eq.6	Vertical from Eq.7	From shear Eq.9
1	10	17	6	3	7	3	8
2.1	6	16	12	4	13	6	14
2.2	7	15	11	4	11	5	13
3	8	24	18	7	19	36	32
4	14	40	34	11	36	53	53
5	41	> 1750	>111	>34	>116		228

Table 15. Second blast test, Leca building. Measured and calculated peak strain.

Blast round	Strain (μstrain)						
	Measured		Calculated based on wave propagation			Calculated from displacement	
	On intact wall	Above door openings	From shear Eq.4	From bending Eq.5	Total strain Eq.6	Vertical from Eq.7	From shear Eq.9
1.1	-	-	3	1	3	-	-
1.2	-	-	5	1	5	2	6
1.3	-	-	10	4	10	3	11
2	11	34	9	3	10	5	18
3	19	87	17	7	18	7	35
4	94	> 3200	75	13	76	306	153

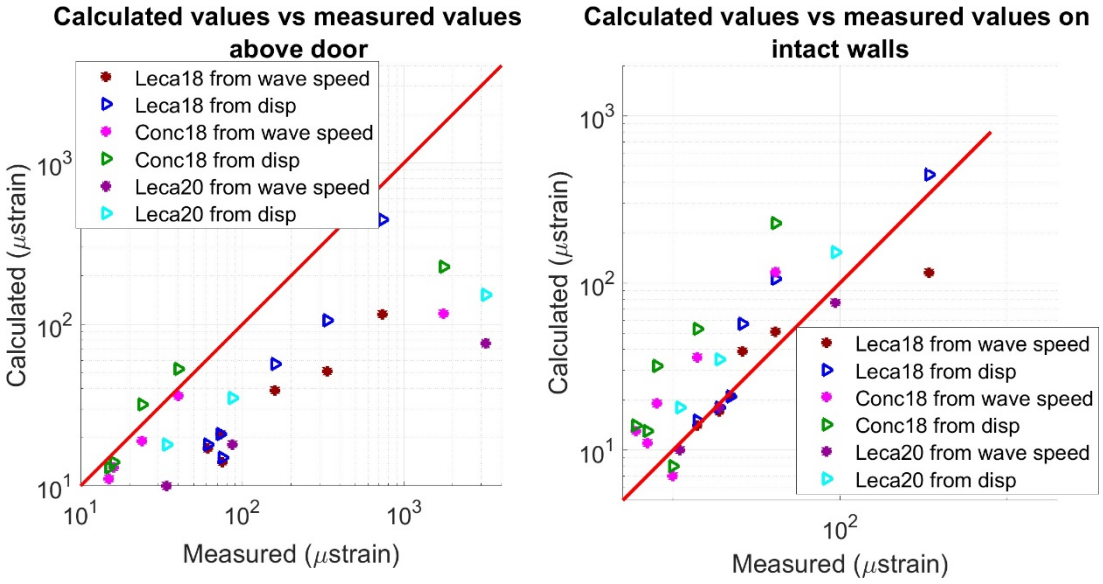

Figure 17. First and second blast test, calculated strain vs left: maximum measured strain (measured above door), right: maximum strain measured on intact walls.

The calculated maximum strain values show good agreement with the measured maximum strain values for the concrete building in the first blast test, while the deviations between measured and calculated maximum strains are large for the Leca buildings in both tests, Figure 17 left. However, both strains calculated based on wave propagation and strains calculated based on displacement estimate the strains in intact, homogeneous walls. Strain (and stress) concentrates in the corners, and these strain concentrations may be large. The highest strains were measured above the door openings. If the calculated strain values are compared to strain measured on the homogeneous side wall and back wall, the compliance is better for the Leca buildings, Figure 17 right.

Strain from shearing calculated from difference in displacement, is higher than total strain calculated based on wave propagation for all test buildings, and the difference is increasing with the blast load. However, strain calculated from difference in displacement include effect of possible building amplification. Further, the strain values calculated based on wave propagation must be considered rough estimates since the wave propagation speed is associated with uncertainty.

Calculated vertical strain based on difference in displacement is higher in the LECA building compared to the concrete building in the first blast test. This can be explained by the fact that the LECA blocks have about ten times lower Young's modulus compared to cast-in-place concrete strength class C30/37 and will react with larger strains when exposed to the same vibration load acting on the foundation. Figure 18 shows displacement time series from blast round 2.1 in the first blast test. The difference between the sensor on top of the wall (V6) and close to the foundation (V7) is clearly larger for the Leca building than for the concrete building.

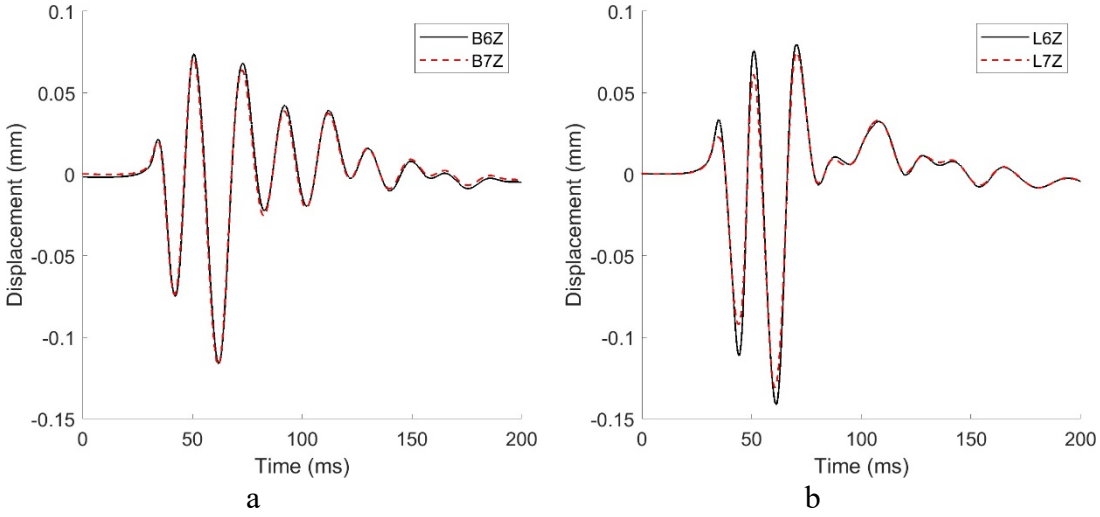

a b

Figure 18. First blast test, vertical displacement from blast round 2 for sensor V6 (near top) and V7 (foundation) on short side facing the blast area. a) Concrete building. b) Leca building

5.2 Vibration frequency

There are several methods to determine the frequency content of a signal. In this study we have determined the frequency content by use of zero-crossing, the response spectrum, instantaneous frequency computed from the Hilbert transform and characteristic frequency calculated from the power spectrum derived from the Fast Fourier Transform (FFT).

The AVA measurement system determines the zero-crossing frequency around each peak in the time series by assuming that the time between the zero-crossing before a

peak and the zero- crossing after a peak corresponds to half a period of the dominant frequency.

The response spectrum, which are often used in earthquake engineering, is calculated from the peak responses of a series of SDOF systems with varying natural frequency, that are forced into motion by the vibration time series. The dominating frequency is determined from the peak in the response spectrum.

The instantaneous frequency, f_{inst}, is computed as the derivative of the phase of the analytic signal found by using the Hilbert transform of the vibration time series, Eq. 10. The analytic signal has a real part which is the original data, and an imaginary part which contains the Hilbert transform. The imaginary part is a version of the original time series with a 90° phase shift. The instantaneous frequency is the time rate of change of the instantaneous phase angle. [7].

$$f_{inst} = \frac{1}{2\pi}\frac{d}{dt}(\arg(z(t))) \qquad (10)$$

where:
z(t) is the analytical signal obtained by Hilbert transform of the original time series.

The characteristic frequency, f_{ch}, is calculated from the Power Spectrum using a maximum-likelihood approach as described in [8].

$$f_{ch} = \sqrt{\frac{m_2}{m_0}} \qquad m_n = \int_0^{f_{max}} f^n S(f) df \qquad (11)$$

where
S is the single sided power spectrum
f is the frequency. The upper frequency is here restricted to 300 Hz in accordance with the measurement range prescribed in [1].

The blast rounds with single charges, delayed by about 3 seconds in between, are well suited for comparison of the different methods, since the vibrations are not affected by interaction between contributions from different detonations. In the first blast test, this was blast round two, with two holes located about 30 m from the measurement position on ground (VZ3). In the second blast test, this was blast round one with three holes located 36 m - 48 m from the measurement position on bedrock below the filling (VZ2) and the closest position in the filling (V14). Note that the detonations in the single blast rounds were constricted by the surrounding rock (no free surface to break against), which may affect the frequency.

Figure 19 shows measured time series from a sensor on bedrock (VZ3 in the first blast test and VZ2 in the second blast test), a sensor on the building close to the building foundation (V7 on concrete building in the first blast test and V13 in the second blast test) and a sensor in the filling in the second blast test (V14).

Figure 20 and Figure 21 show the Response spectra, PSD from FFT and the zero-crossing frequencies determined by the measurement system for the same time series. Response spectra and PSD are determined using the entire time series, while the Hilbert frequency is calculated around the maximum peak in the time series (between the dashed lines in Figure 19). Zero-crossing frequencies for all peaks above PPV = 1.0 mm/s are shown in the figures.

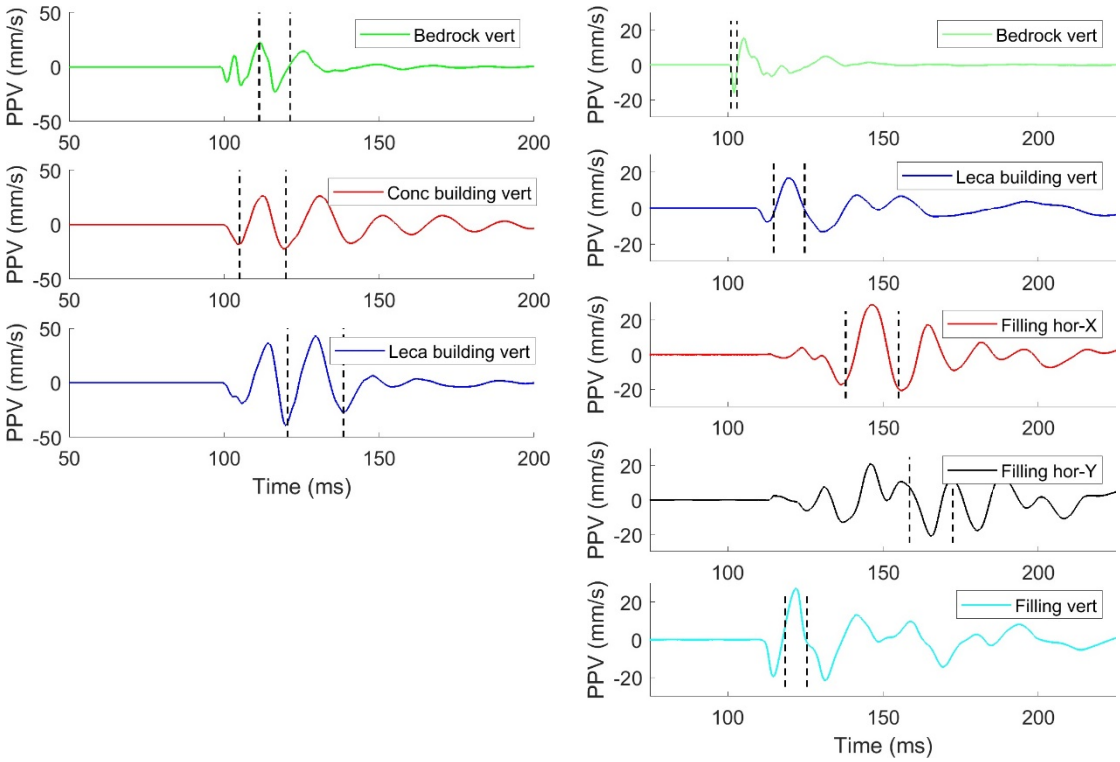

Figure 19. First and second blast test, measured vibration velocity from single blast rounds. The part of the time series used in the calculation of the instantaneous frequency by use of the Hilbert transform are between the dashed lines. Left: First blast test, blast round 2.1, time series from vertical sensor on bedrock, VZ3, and vertical sensors on buildings, V7. Right: Second blast test, blast round 1.3, time series from vertical sensor on bedrock below filling (VZ2), vertical sensor on building, (V13), and vertical and horizontal sensors in filling (V14).

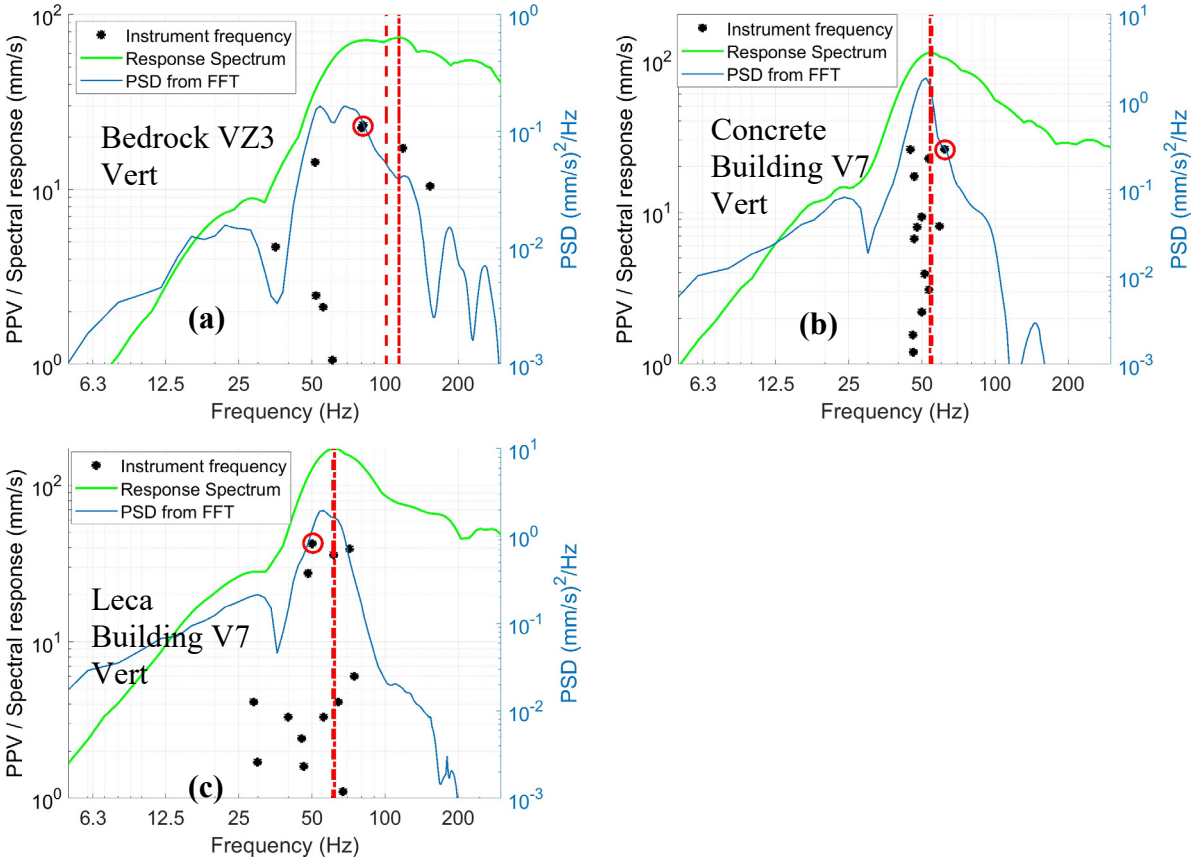

Figure 20. First blast test, measured vibration velocity in vertical direction from the single hole blast round 2.2. Peak values vs frequency determined by the measurement system (zero-crossing), response spectra and PSD from FFT. The frequencies reported in Table 16 are marked with circles (zero crossing around max peak), dashed lines (characteristic frequency from PSD) and dashed-dotted lines (peak in response spectra). a) sensor VZ3 on bedrock, b) sensor V7 on concrete building, c) sensor V7 on Leca building.

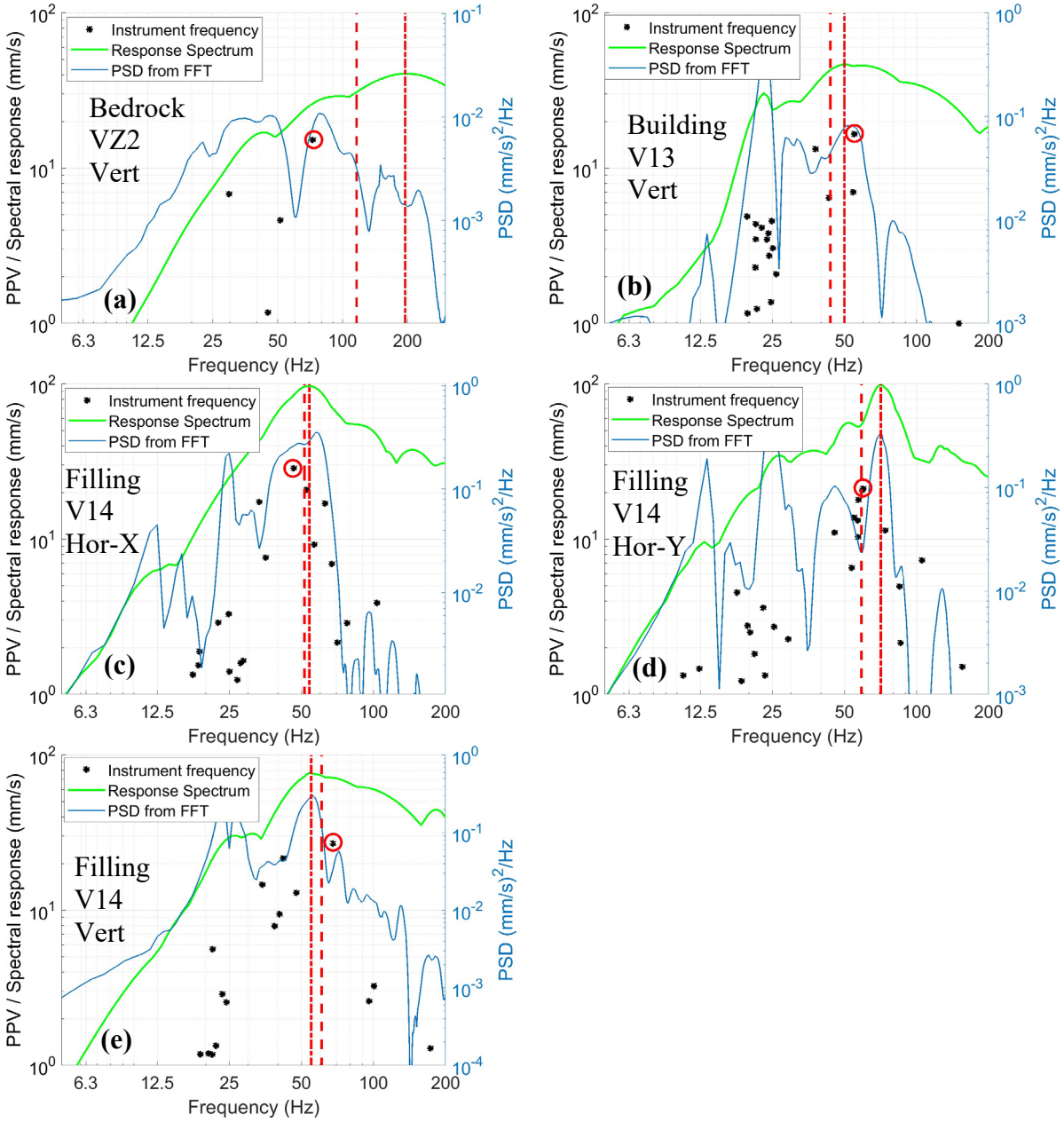

Figure 21. Second blast test, measured vibration velocity from the single hole blast round 1.3. Peak values vs frequency determined by the measurement system (zero-crossing), response spectra and PSD from FFT. The frequencies reported in Table 16 are marked with circles (zero crossing around max peak), dashed lines (characteristic frequency from PSD) and dashed-dotted lines (peak in response spectra). a) sensor VZ2 on bedrock. b) sensor V13 on building. c) sensor V14 in filling horizontal x-direction. d) sensor V14 in filling horizontal y-direction. e) sensor V14 in filling vertical direction.

For the blast rounds that involves several holes with a delay between each hole, the measured time series become more complex, and it is more difficult to describe the

frequency with a single number. For the third blast round in the first blast test, shown in Figure 22, the chosen delay interval, 10 ms, clearly affects the frequency by introducing a strong frequency component around 100 Hz. Furthermore, the zero-crossing frequency determined by the instrument around the maximum peak value deviates considerably from the frequency range where most of the vibration cycles have their zero-crossing frequency. In these circumstances, the use of a single frequency value gives a poor description of the frequency content and demonstrates the difficulty of using frequency dependent limit values, such as in the British and American Standards. This is because a frequency dependent limit value requires that all frequencies with corresponding amplitudes from the blast are determined and compared to the limit value curve, and not just the frequency of the cycle with highest peak value, as many instruments provide as the only output. An alternative approach is to implement a frequency weighting filter that directly considers the damage potential at different frequencies.

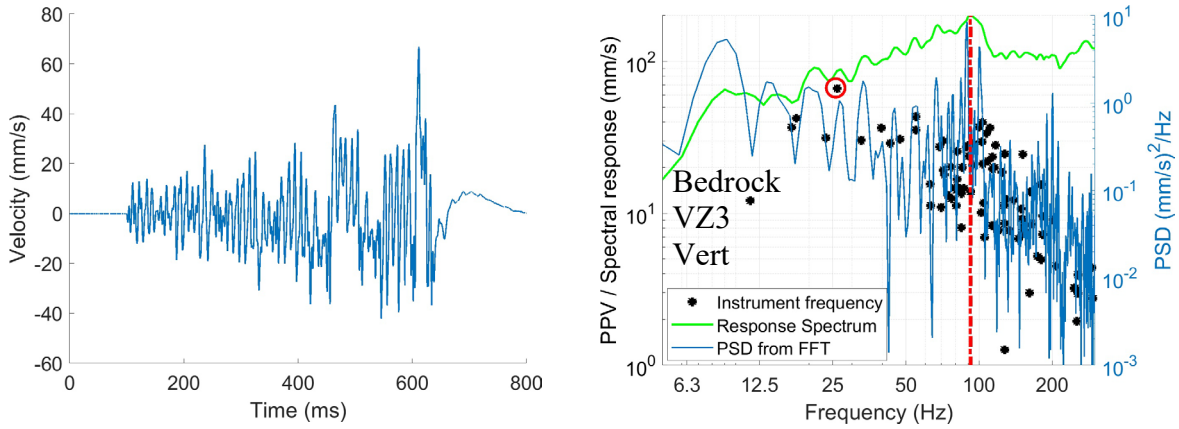

Figure 22. First blast test, measured vibration velocity from third blast round. Sensor on ground, VZ3. Left: Time series. Right: Peak values vs frequency determined by the measurement system (zero-crossing), response spectra and PSD from FFT. The frequencies selected for reporting in Table 16 are marked with circle (zero crossing around max peak), dashed line (characteristic frequency from PSD) and dashed-dotted line (peak in response spectra).

Table 16 shows the vibration frequencies determined for the sensors on bedrock and filling for all blast rounds using the following methods: frequency determined by the measurement system (zero crossing around the maximum peak), peak in response spectra, instantaneous frequency determined by the Hilbert transform and characteristic frequency of the power spectrum from FFT. In addition, results for one sensor on the test building for blast 2.2 in the first blast test and blast 1.3 in the second blast test are shown.

Table 16. First (2018) and second (2020) blast tests, vibration frequencies determined by use of different methods.

Blast round	Hor dist (m)	Pos/Sensor	Dir	Instrument frequency (zero crossing around highest peak) (Hz)	Instantaneous frequency from Hilbert transform (Hz)	Peak in response spectrum (Hz)	Characteristic frequency from FFT (Hz)
1-2018	35	VZ3 / Bedrock	Vert	100	95	102	117
2.1-2018	33			65	87	117	99
2.2-2018	30			81	84	114	101
3-2018	23			26	32	92	93
4-2018	18			41	45	83	97
5-2018	14			21	20	20	45
2.2-2018	24	V7 / Conc build	Vert	62	62	54	54.7
	27	V7 / Leca build		50	50	62	61
1.1-2020	52	VZ2 / Bedrock	Vert	64	238	88	110
1.2-2020	46			93	202	90	121
1.3-2020	40			72	228	195	116
2-2020	37			213	199	181	105
3-2020	22			144	141	196	156
4-2020	12			163	155	118	126
1.3-2020	36	V13 / Leca build	Vert	55	55	50	44
1.3-2020	35	V14 / Filling	Hor-X	47	46	54	52
2-2020	31			44	43	41	49
3-2020	16			35	33	45	39
4-2020	6.4			11	9	10	33
1.3-2020	35		Hor-Y	60	63	71	59
2-2020	31			39	39	43	41
3-2020	16			11	11	16	27
4-2020	6.4			9	14	9	38
1.3-2020	35		Vert	68	59	55	61
2-2020	31			71	66	63	76
3-2020	16			29	30	105	63
4-2020	6.4			15	12	23	44

5.3 Vibration frequency versus charge and distance

The results in Table 16 indicates a reduction of the dominant frequency with decreasing distance. This is not in accordance with the assumptions behind the distance factor in the Norwegian Standard and else reported in literature. However, this finding can be explained by the fact that the blast tests were designed to produce increasing vibration values, which was achieved by both increasing the charge weights and reducing the

distance for each blast round. To obtain a clearer picture of the effect of distance and charge weight, frequency and distance can be scaled with the charge weight as described in [9] and [10], using the following equations:

$$d_{sc} = \frac{d}{\sqrt{Q}} \quad (12)$$

$$f_{sc} = f\sqrt{Q} \quad (13)$$

Where:
d_{sc} = scaled distance (m/kg$^{0.5}$)
f_{sc} = scaled frequency (Hz·kg$^{0.5}$)
d = distance (m)
f = frequency (Hz)
Q = maximum charge/ delay (kg)

In Figure 23 scaled instrument frequency (zero-crossing frequency around highest peak) is plotted against scaled distance for all blast rounds and sensors in both blast tests. A clear tendency towards reduced scaled frequency with increased scaled distance can be seen. This agrees with what is reported in e.g. [11].

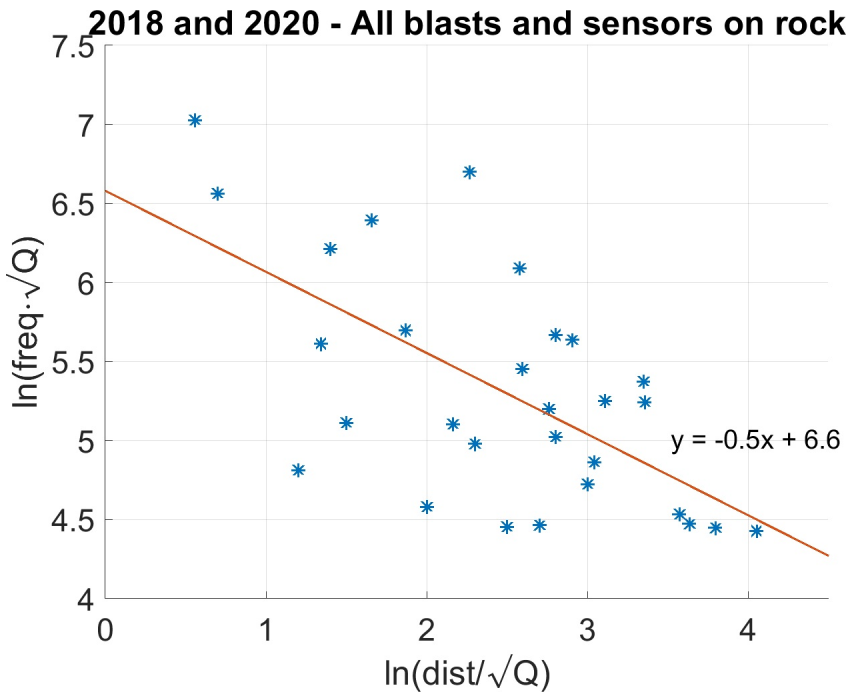

Figure 23. First and second blast tests, scaled instrument frequency versus scaled distance.

5.4 Building natural frequencies and amplification

Excitation close to the building's natural frequencies can cause high strains because of amplification of the vibrations and that different building parts can vibrate out of phase or move relative to each other. The building's natural frequencies occur in the whole frequency range, but the fundamental frequencies are the most important since they have largest amplitude and causes the highest strain. According to [12], they are usually found in the frequency range from about 4 Hz to 15 Hz. In [13] fundamental resonance frequencies between 5-10 Hz were reported.

Figure 24 shows the response of the test buildings in the first blast test to hammer excitation and to the single hole blasts (blast round two). The peaks in the response from hammer excitation and from blast excitation are rather consistent, but with slightly higher frequencies for the hammer excitation in the horizontal Y-direction, in which the buildings are stiffest. This is probably because the hammer excitation fails to excite the entire structure in the Y-direction.

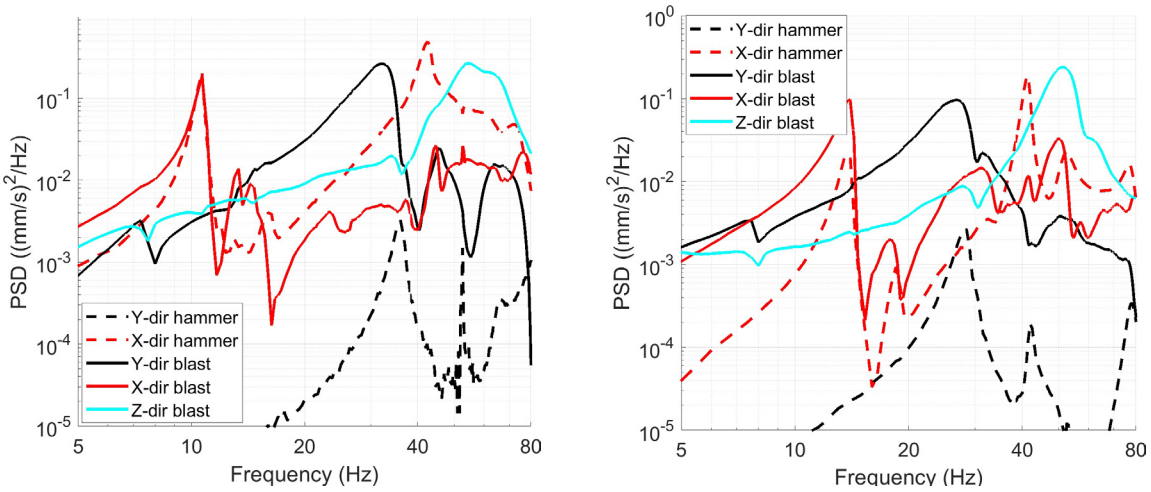

Figure 24. First blast test, building response (PSD) from hammer and blast excitation. Left: Leca building, right: Concrete building. See Figure 5 for *coordinate system.*

Figure 25 left shows the response of the test building in the second blast test to hammer excitation and to the single hole blasts (average of blast 1.1, 1.2 and 1.3). The natural frequencies of the building are not as clearly seen as in the first blast test, as the dynamics of the filling also affects the building response. A comparison between the response of the building and the response of the filling show that the peaks in the frequency spectra of the building and filling coincide at about 11-13 Hz and at about 23-25 Hz. However, the peak at 7 Hz in X-direction cannot be seen on the filling.

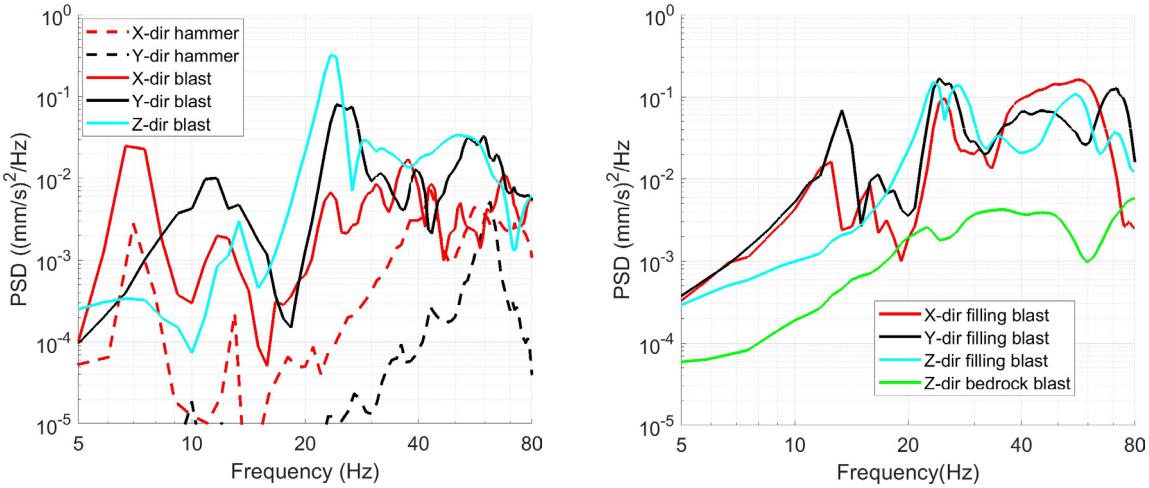

Figure 25. Second blast test, building response (PSD) from hammer and blast excitation. Left: Leca building, right: Filling and bedrock below filling. See Figure 9 for coordinate system.

A clearer picture may be obtained by looking at the Frequency Response Functions (FRF) between measured response on the building/filling and measured response on bedrock below the filling. The FRF is determined according to Eq. (14) from Ref. [14].

The coherence determined according to Eq. (15) provides a measure of the extent to which the response measured on the building/filling are caused by the blast and not by other unrelated sources. The coherence is between zero and one. A coherence equal to one implies that the vibrations originates fully from vertical vibrations in bedrock below the filling and a coherence close to zero that the vibrations may be caused by other unrelated sources.

$$\hat{H}(f) = \frac{\hat{S}_{yx}(f)}{\hat{S}_{xx}(f)} \tag{14}$$

$$\hat{\gamma}_{xy}^2(f) = \frac{|\hat{S}_{yx}(f)|^2}{\hat{S}_{xx}(f)\hat{S}_{yy}(f)} \tag{15}$$

where

$\hat{H}(f)$ is the average frequency response function from vibration in bedrock below the filling and vibrations on building/filling

$\hat{\gamma}_{xy}^2(f)$ is the coherence between vibrations in bedrock below the filling and vibrations on building/filling

$\hat{S}_{yx}(f)$ is average of the cross spectral density between vibrations in bedrock below the filling and vibrations on building/filling from blast 1.1, 1.2 and 1.3.

$\hat{S}_{xx}(f)$ is the average of auto spectral density of the vibrations in bedrock below the filling from blast 1.1, 1.2 and 1.3

$\hat{S}_{yy}(f)$ is the average of auto spectral density of the vibrations on building/filling from blast 1.1, 1.2 and 1.3

Figure 26 upper panels show the the frequency response functions and the lower panels show the coherence. The results indicate that the identified peak in X-direction at 7 Hz in Figure 25 corresponds to the buildings first natural frequency, since a peak can only be seen in the FRF of the building in X-direction and not in the FRFs for the filling in any of the directions. The peaks at 11-13 Hz and at 23-25 Hz in Figure 25 corresponds to peaks in the FRF of the building and filling in the horizontal and vertical direction respectively. This indicates that these are the natural frequencies of the combined system of building on filling.

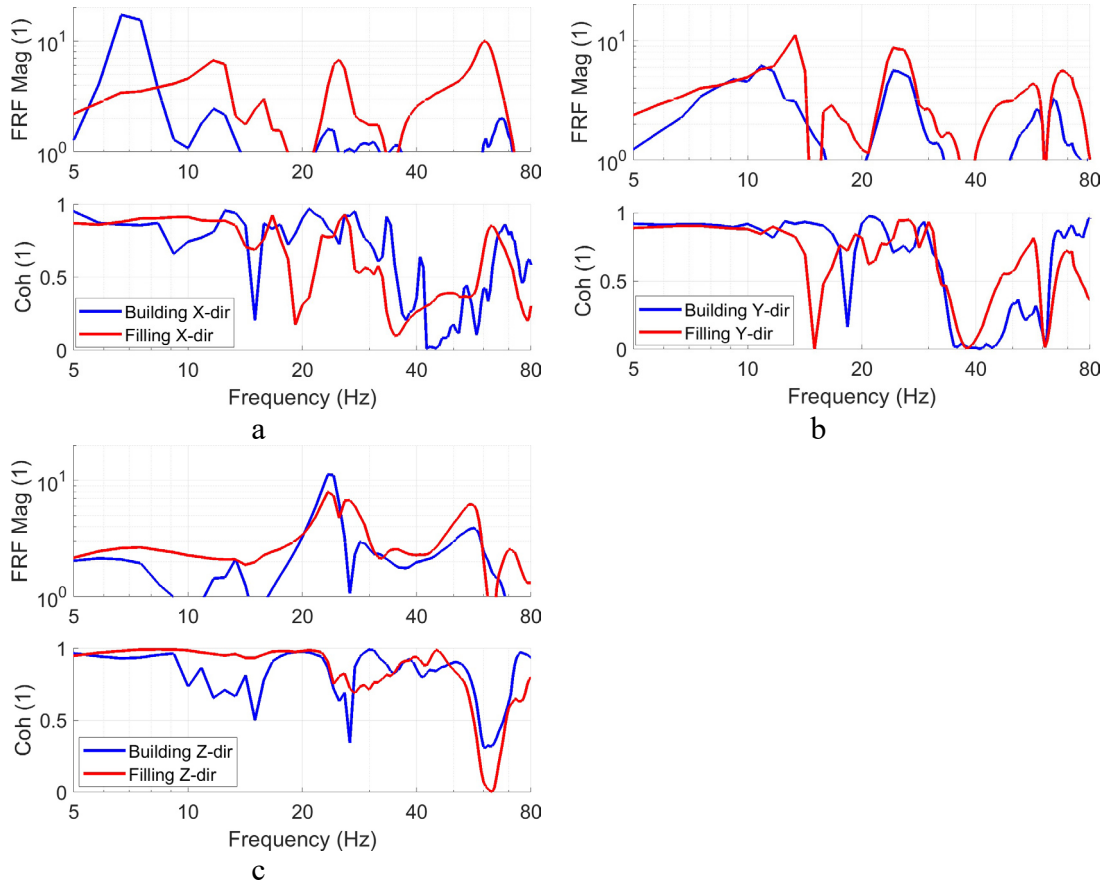

Figure 26. Second blast test, Frequency response function (FRF) between sensors on building/filling and vertical senor below filling (VZ2). Calculated from blast 1.1, 1.2 and 1.3. a) Horizontal x-direction. b) Horizontal y-direction. c) Vertical z-direction. See Figure 9 for coordinate system.

Table 17 shows the natural frequencies for the test buildings in the first and second blast test. The natural frequencies for the test buildings in the first blast test are higher than reported in [13]. This can be explained by the fact that the test buildings' dimensions were reduced compared to normal buildings. This natural frequency of the Leca building on filling in the second blast test are lower than for the Leca building in the first blast test and more in agreement with what is reported in [13].

Table 17. 1st First (2018) and second (2020) blast test, natural frequencies for the test buildings

Building	Dimensions (l·w·h)	Foundation	1st resonance frequency (Hz)	
			X-normal to long side	Y-normal to short side
Concrete - 2018	5 x 2 x 2.4	Wall footing on thin compacted layer of gravel over rock	14	28
Leca - 2018			11	36
Leca - 2020	7 x 3 x 2.4	Wall footing on filling	7	11

Figure 27 left shows the amplification factors from foundation level (vertical direction) to structure (position and direction with max PPV). Figure 27 right plots the amplification factors against dominating frequency at ground below the structures (measured in VZ3 on bedrock in first blast test and in pos 14 in the filling in the second blast test.

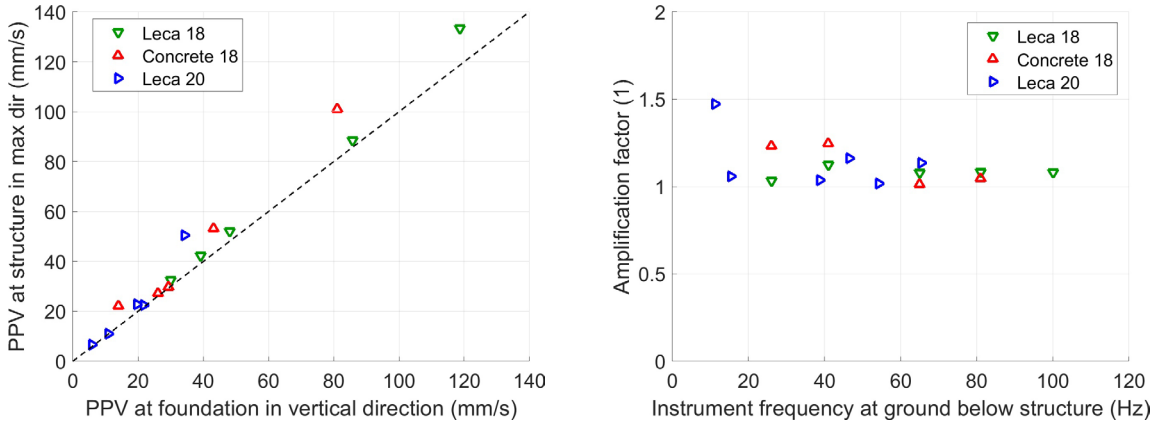

Figure 27. First and second blast tests. Left: measured PPV on structure (position and direction with max PPV) versus measured PPV on structure in vertical direction at foundation level. Right: amplification factors from foundation (vertical direction) to structure (position and direction with max PPV) versus dominating frequency at ground below the structures (measured on bedrock in first blast test and in filling in the second blast test)

The amplification factors in Figure 27 are in accordance with the findings in [13], which reported little or no amplification in structures from ground motions above 45 Hz. However, the amplification factors are lower than reported in [15], and there seems to be less correlation between the frequency and the amplification factor compared to the results in [15]. This can be explained by the fact that the measured frequencies around the peak values, Table 16, are considerably higher than reported in [15], where large charges and long distances gave frequencies in the range of typical building resonances. This is especially true for the first blast test. For the second blast test, measured frequency in the filling was lower than on bedrock below and a slight correlation between building amplification factors and frequency can be seen in Figure 27 right.

5.5 Vibration velocity vs charge

An attempt has been made to attribute specific part of the time series to explosion in individual boreholes in the first blast test. Propagation speed for P- and R-waves were varied until best possible match were obtained. The same wave propagation speed was used for all bore holes. It is noted that the stated delay time of 10 ms leads to a too short vibration event compared to the measured time series for all blast rounds. Therefore, the delay time was adjusted to 10.2 ms in the calculations, to obtain arrival of the first and last vibration wave at the same time as the first and last peak in the time series. Figure 28 shows measured velocity on bedrock in position VZ3 from blast round 3 together with calculated arrival time for P- and R- waves from the individual bore holes. Distance to the individual bore holes and the corresponding scaled charge ($\sqrt{Q}/d$) are also shown in the figure. An exact fit cannot be obtained, probably because of varying wave propagation speed between the holes and interference between vibration waves from different bore holes. The figure shows that the highest peak velocity occurs close to the largest scaled charges, as expected. However, there does not appear to be a linear correlation between scaled charge and measured velocity. This is probably due to local variations in propagation conditions, e.g. occurrence and direction of cracks as well as interference between vibration waves from different bore holes.

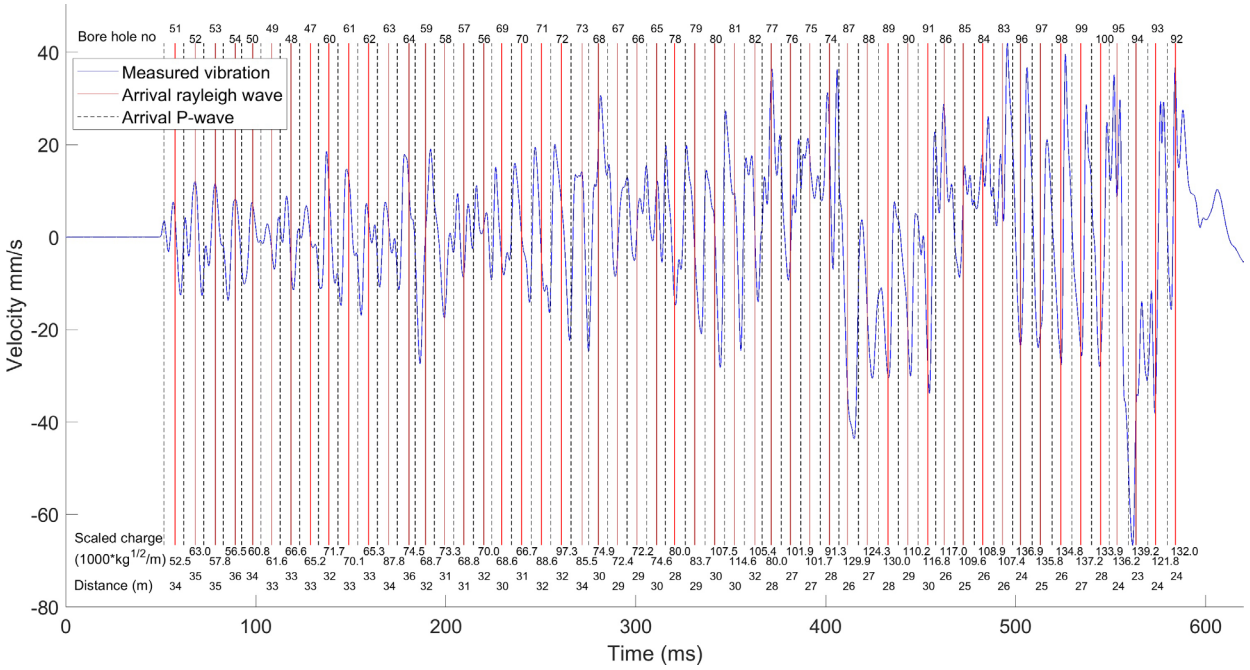

Figure 28. First blast test, blast round 3, measured vibration velocity on bedrock (in VZ3) and calculated arrival time of P- and R-waves from individual bore holes, see Figure 14 for localisation of bore holes.

5.6 Measurement on cladding and composite walls versus solid walls

Table 18 shows measured PPV in vertical direction on cladding, V9, (see Figure 8d) and in vertical direction on concrete wall, V7, for all blast rounds in the first blast test. Example of time series and corresponding PSD from the two sensor positions are shown in Figure 29. Measured PPV is higher on the cladding for all blast rounds. The amplification factor from concrete wall to cladding is between 1.4-1.8. The PSD in Figure 29 shows that measured vibrations velocity on the cladding is higher than on the concrete in the frequency range above 20 Hz, with the largest difference for frequencies above 100 Hz. The results indicate that measurements on cladding do not give results that are representative for the vibrations in the walls behind.

Table 18. First blast test, measured PPV in vertical direction on concrete wall (V7) and on cladding (V9).

Blast round	PPV (mm/s)		Amp factor concrete-cladding
	Concrete	Cladding	
1	14	25.3	1.8
2.1	29.1	41.8	1.4
2.2	26.3	40.9	1.6
3	42.8	61.2	1.4
4	80	145.9	1.8
5	>262	>262	-

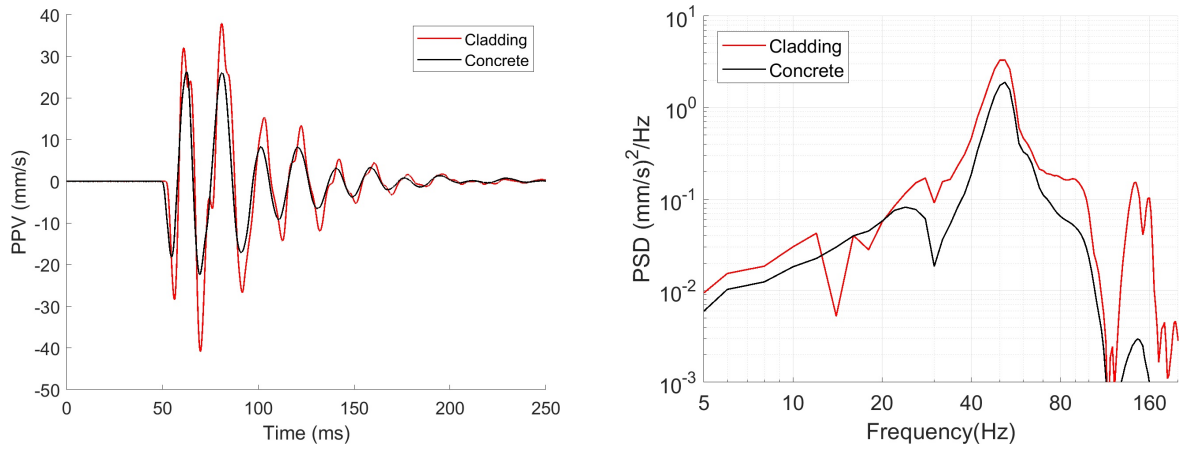

Figure 29. First blast test, blast round 2, measured vibration velocity in vertical direction on concrete wall (V7) and on cladding (V9). Left: Time series. Right: PSD. See Figure 7 for sensor positions.

Table 19 shows measured PPV in vertical and horizontal X-direction on an insulated block (VZ1/A1) and on a standard Leca block (V10/A2), for all blast rounds in the

second blast test. Example of time series and corresponding PSD from the sensor positions are shown in Figure 30.

The measured PPVs in vertical direction are slightly higher on the insulated block for all blast rounds except the last blast round. The amplification factor from the standard Leca block to the insulated block is between 0.9-1.3. The PSD in Figure 30 shows that the measured vibrations velocity in vertical direction on the insulated block and on the standard Leca block are very similar in the whole frequency range. The results from the two sensors in horizontal direction deviates slightly more and especially above 40 Hz.

The results indicate that measurements in vertical direction on insulated blocks give similar results as measurements on standard Leca blocks. However, at short distances, when horizontal measurements are relevant, care must be taken.

Table 19. Second blast test, measured PPV in vertical direction on insulated block (VZ1) and on standard Leca block (V10).

Blast round	Vertical PPV (mm/s)		Amp factor	Horizontal PPV (mm/s)		Amp factor
	Standard Leca	Insulated block		Standard Leca	Insulated block	
1.1	5.2	6.2	1.2	1.9	1.8	0.9
1.2	9.0	10.3	1.1	3.6	3.3	0.9
1.3	19.0	18.6	1.0	5.7	4.2	0.7
2	21.8	23.0	1.1	10.0	12.0	1.2
3	23.1	24.1	1.0	13.0	17.5	1.3
4	131.8	121.7	0.9	63.6	63.7	1.0

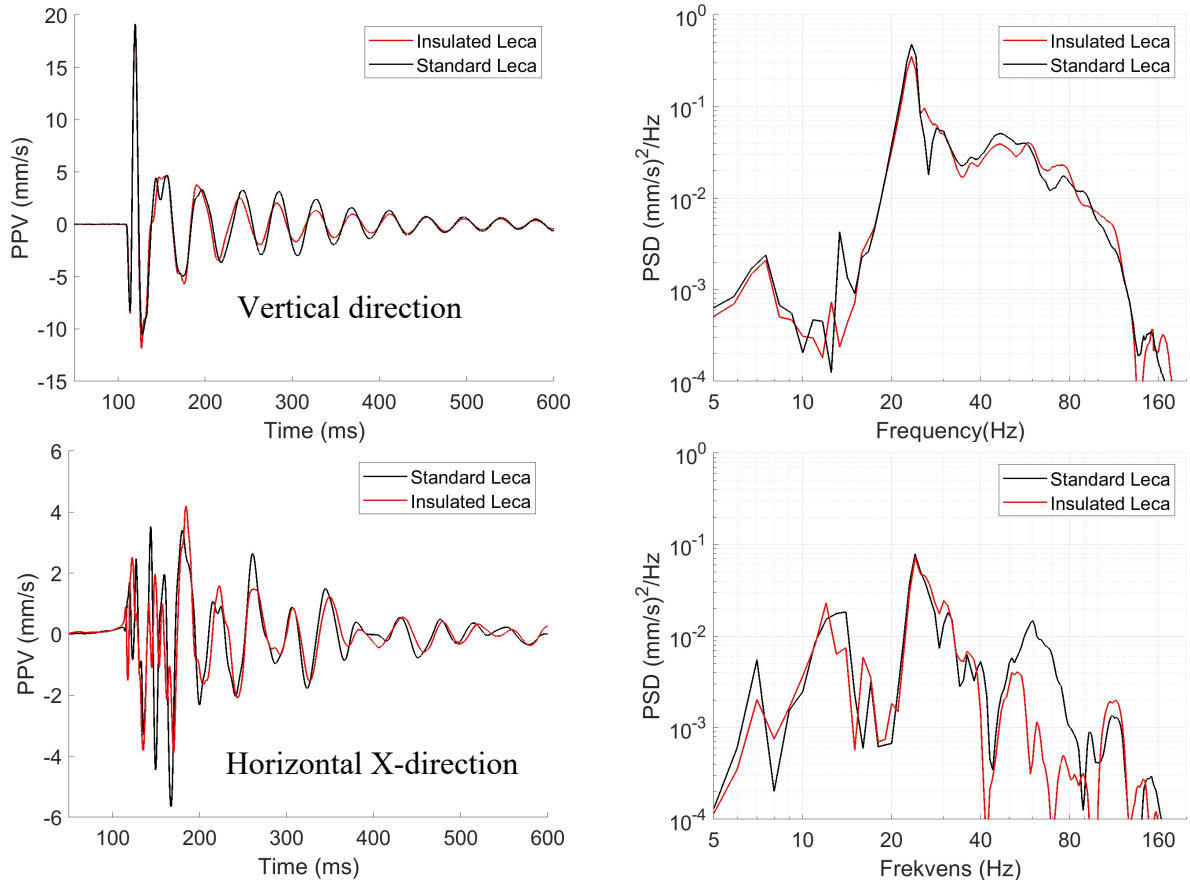

Figure 30. Second blast test, blast round 1.3, measured vibration velocity on a standard Leca block and on an insulated block. Top: vertical direction (sensor VZ1 and V10). Bottom: horizontal X-direction (sensor A1 and A2). Left: Time series. Right: PSD. See Figure 9 for sensor positions.

6 Discussion

Both blast tests produced vibration values well above the limit values in today's Norwegian standard. Despite this, no visible damage was found on any of the buildings. The buildings were however exposed to strain levels which are above the critical strain levels discussed in [13]. This may indicate that these newly erected constructions may tolerate higher strain levels than what has been found to produce cracking in other studies. Cured, but still young and flexible concrete and mortar, may get more brittle during further curing. In addition, drying makes permanent tension stresses develop over time.

The present study was designed to investigate damages to outer walls. According to [13] the inner division wall and ceiling material are often the most vibration sensitive parts of the building, especially old plaster and lath walls. This needs to be taken into consideration before the limit values may be adjusted.

The relatively high resonance frequencies of the test buildings compared to more common buildings, may have affected the vibration response, especially in the first blast test. For damage mechanisms like shearing and bending, for which the building is forced to follow the vibration motion of the ground surface, the deviation in resonance frequencies is of minor concern. However, since measurements in accordance with most national standard are specified to be carried out at foundation level, building amplification may be higher in more common buildings than in the test buildings in this experiment. This may cause resonant response to become a more dominant damage mechanism in more common buildings. This needs to be taken into consideration before the limit values may be adjusted.

7 Conclusions

These field blast experiments have contributed to increased understanding of vibration generation and propagation from bench blasting in rock, response of buildings to ground vibration and vibration damage mechanisms for concrete and light weight aggregate masonry buildings. Two extensive set of high-quality synchronized vibration- and strain measurement data are made available, from a series of well controlled, well documented rock blast rounds.

Strain calculated from shear wave velocity in ground, measured PPV and frequencies on the buildings as well as difference in displacement, agrees fairly well with strain measured on the homogeneous walls.

Dominant frequencies of the vibrations determined by different methods show a considerable deviation, with a distinct difference between methods which determine the frequency in a short time interval around the highest peak and methods which are using the entire vibration time series. Further, methods which determines the frequency in short time intervals show a large spread in the frequency between the different vibration cycles. This points to the difficulty of using frequency dependent vibration limit values.

Measurements on cladding do not appear to give results that are representative for the vibrations in the walls behind the cladding, while vertical measurements on insulated blocks appear to give the same results as measurements on standard Leca blocks. However, at short distances, when horizontal measurements are relevant, care must be taken.

The first blast tests produced vibration values above PPV = 260 mm/s and the second blast tests a maximum PPV = 180 mm/s. These results are well above the vibration limit values calculated according to today's Norwegian standard, which are 50 mm/s for the test buildings in the first blast test and 16-23 mm/s for the test building in the second blast test. The maximum measured strain levels were > 1750 μstrain in the first blast test and > 3200 μstrain in the second blast test. This is above critical strain levels reported

in earlier studies. Despite this, no visible damage could be detected either on the walls or on tiles in any of the test buildings.

The results of the two blast tests indicate that today's limit values include a large safety margin for buildings on rock and well compacted stiff soil, when considering damages to outer walls, which this study was designed to investigate.

8 References

[1] NS 8141:2001 Vibration and shock. Measurement of vibration velocity and calculation of guideline limit values in order to avoid damage on constructions. (In Norwegian)

[2] SINTEF Byggforsk rapport 18141BM Prøvningrapport Bergmekaniske egenskaper. Test av borekjerner boret normalt på/parallel med foliasjon fra testsprengningsområde Solør vgs. Avd Våler Steinbrudd, Spjulsåsen. 2019-01-17

[3] Bonnefoy-Claudet, S., Cornou, C., Bard, P.Y., Cotton, F. Moczo, P., Kristek, J., Fäh, D. H/V ratio: a tool for site effects evaluation. Results from 1-D noise simulations. Geophys. J. Int. (2006) 167, 827-837

[4] http://www.micronoptics.com/wp-content/uploads/2018/01/os3510-1.pdf

[5] Rathje E.M., Chang W.J., Stokoe K.H., Cox B.R. Evaluation of ground strain from in situ dynamic response. 13th World Conference on Earthquake Engineering Vancouver, B.C., Canada August 1-6, 2004 Paper No. 3099.

[6] Remedy deliverable 4.1 Vibration induced damage due to construction work – State of the Art Report. Rev 0, 07/2019

[7] https://se.mathworks.com/help/signal/ug/hilbert-transform-and-instantaneous-frequency.html

[8] Cartwright, D.E. and Longuet-Higgins, M.S. The statistical distribution of the maxima of a random function. Proceedings of the Royal Society of London, Series A, Vol. 237, 1956.

[9] Ambraseys, N. and Hendron, A. Dynamic Behavior of Rock Masses. In K. Stagg, & O. Zienkiewicz, Rock Mechanics in Engineering Practice (pp. 203-236). London: John Wiley & Sons (1968).

[10] Baker, Westine and Dodge. Similarity Methods in Engineering Dynamics – Theory and Practice in Scale Modelling – Revised Edition. Elsevir (1991)

[11] Liu D, Lu W., Liu Y., Chen M., Yan P., Sun P. Analyse of the main factors influencing the dominant frequency of blast vibration. Hindawi Shock and Vibration Volume 2019, Article ID 8480905 https://doi.org/10.1155/2019/8480905

[12] BS 7385-2:1993 Evaluation and measurement for vibration in buildings – Part 2: Guide to damage levels from groundborne vibration

[13] Siskind, D.E., Stagg, M.S., Kopp J.W., and Dowding C.H. Structure response and damage produced by ground vibration from surface mine blasting. Report of investigations 8507, US Department of Interior, Office of surface mining Reclamation and Enforcement, 1983.

[14] Brandt, A., Noise and Vibration Analysis. Signal Analysis and Experimental Procedures. John Wiley & Sons, Ltd (2011).

Singh, P.K., Roy, M.P. Damage to surface structures due to blast vibration. International Journal of Rock Mechanics & Mining Sciences 47 (2010) 949-961.

REMEDY
Et BegrensSkade prosjekt

Review and reference page

Document information		
Deliverable title Vibration induced damage due to construction work – Blasting tests		***Deliverable No.*** D4.2
Work package No. 4	***Distribution*** Open	***Date*** 2021-12-01
		Rev. No and date 1.0
Client The Research Council of Norway		
Keywords Vibration, damage, blast, ground work, landslide		

Document control

Quality assurance according to **NS-EN ISO9001**

Rev.	***Reason for revision***	***Self review by:***		***Colleague review by:***		***Independent review by:***		***Inter-disciplinary review by:***	
0.1	Draft	KNC	27/9-19	CM	22/8-19				
1.0	Original document	KNC	01/12-21	Nils Ramstad	25/11-21				